University of Groningen
Physics

Modelling the Tau lepton decay

Thijs Rozeboom (S3795837)
First examiner: Kristof De Bruyn
Second examiner: Ema Dimastrogiovanni

July 3, 2023

Abstract

In this report the preliminary results of the feasibility study aimed at measuring the $B_c^+ \to (\tau^+ \to \pi^+\pi^+\pi^-\nu_\tau)\nu_\tau$ decay was improved upon by including the resonance structure of the τ particle, which decays as $a_1(1260) \to \pi^+(\rho^0 \to \pi^+\pi^-)$. As within the analysis of the preliminary results, a multivariable analysis is performed (MVA). An MVA allows for a quantification of the accuracy of distinguishing the signal decay from background decays. The MVA acquired from the preliminary results is, in this report, referred to as the original MVA. Adding the resonance structure of the τ particle to the considered decay results in a decrease in the significance of 0.94σ resulting when fitting with the original MVA, which was trained on PHSP data. The original MVA was shown to perform similarly to an MVA which was trained on data that includes the resonance structure of the τ particle. This resulted in the inclusion of the mass of the three pions as observable on which the MVA is trained to possibly improve its performance. This required an improved description of the $B^+ \to \bar{D}^0\pi^+\pi^+\pi^-$ and $B^+ \to \bar{D}^{0*}\pi^+\pi^+\pi^-$ decays as was shown, that the MVA otherwise distinguishes on the presence of the τ resonance structure in the decay. As two descriptions for the $B^+ \to \bar{D}^{0*}\pi^+\pi^+\pi^-$ where possible, both were used separately to allow comparison. Resulting in two MVAs that gave significance for the $B_c^+ \to \tau^+\nu_\tau$ decay of 3.07σ and 2.47σ. This shows a need to use both descriptions when describing $B^+ \to \bar{D}^{0*}\pi^+\pi^+\pi^-$. When comparing this to the original MVA significance of 3.51σ it shows that the end result of this report resulted in a decrease of the significance of 0.44σ and 1.04σ. From this, it can be concluded that further improvements are necessary in order to claim the measuring of the $B_c^+ \to \tau^+\nu_\tau$ decay when analyzing real data.

Contents

1 Introduction

The behaviour of the fundamental particles and three of the fundamental forces are described by the Standard Model (SM). The name SM was first introduced by Abraham Paris and Sam Treiman in 1975. [1] Since its introduction, the SM has been widely successful in explaining experimental observations and accurately predicting a wide variety of phenomena [2].

Although the SM has been wildly successful it has discrepancies when describing certain physical phenomena. These discrepancies prompted the High Energy Physics (HEP) community to research these discrepancies resulting in theoretical models commonly known as Physics beyond the Standard Model (BSM). One physical phenomenon that would result in BSM is the violation of lepton flavour universality (LFU). LFU refers to the electroweak coupling of leptons to gauge bosons where the coupling is independent of their respective flavour. [3] Recent studies on the transition $b \to c\ell^-\bar{\nu}_\ell$ in the $\mathcal{R}(D)$ and $\mathcal{R}(D^*)$, show an enhanced ratio of 1.4σ and 2.8σ respectively, when compared to the SM. This resulted in a combined difference of 3σ which hints that LFU symmetry may be broken. [4]

To acquire further insight into this deviation, the $B_c^+ \to \tau^+\nu_\tau$ decay can be studied. The $B_c^+ \to \tau^+\nu_\tau$ decay regards the quark transition $\bar{b}c \to \ell^+\nu_l$ which is on the quark level identical to $b \to c\ell^-\bar{\nu}_l$. Currently no branching fraction of the $B_c^+ \to \tau^+\nu_\tau$ has been measured, but by use of the Large Hydrogen Collider beauty (LHCb) located at the European Organization for Nuclear Research (CERN) the branching fraction can possibly be measured.

Preliminary results of measuring the $B_c^+ \to \tau^+\nu_\tau$ decay, acquired by J. R. de Jong [5], uses the three pions that result from the $\tau^+ \to \pi^+\pi^+\pi^-\nu_\tau$ decay to reconstruct the decay. This is done as the $B_c^+ \to \tau^+\nu_\tau$ decay includes a ν_τ, which can not be measured. Due to this missing information, the B_c^+ decay vertex can not be reconstructed. Resulting in an analysis that uses measured hits to identify the decay. Within the work of J. R. de Jong [5] this analysis has shown to lead to positive results.

However, the current study makes use of the RapidSim library to generate its events. [6] RapidSim is a Monte Carlo (MC) event generator that simulates a phase space decay. It is capable of generating thousands of events in a matter of seconds by approximating the detector response. As RapidSim is a PHSP event generated, this means that the well-known resonance particle of the τ decay is not taken into consideration. This thesis will build on the feasibility test to measure the $B_c^+ \to \tau^+\nu_\tau$ decay by considering the resonance structure of the involved τ particle. This resonance structure is introduced by making use of an MC library called Tauola, further described in Sec.5.2, which is specifically designed to describe τ particle decays.

The full decay of $\tau^+ \to \pi^+\pi^+\pi^-\nu_{\bar{\tau}}$ is given by $\tau^+ \to \nu_{\bar{\tau}}(a_1^+(1260) \to \pi^+(\rho^0 \to \pi^+\pi^-))$. From this, it is easy to see that the introduction of the resonance structure will affect the mass spectrum of the three pions, causing its distinction from other background decays to also change. The purpose of this analysis is to visualize this effect. For this purpose, the already-established multivariate analysis, introduced in Sec.4.3, with the required observables, discussed in Sec. 4.2, are used.

The remainder of this report describes the following: Sec. 2 and Sec. 3, introduce needed background information. In Sec. 4 the framework of the feasibility, by which the preliminary results are acquired, is established. This is followed, in Sec. 5, by a description of the simulation framework used in this analysis. Sec. 6 discusses the effect of the resonance structure on the observables that are considered. Sec. 7 discusses the effect of the resonance structure on the results of the feasibility study. In Sec. 8 further improvements are introduced, worked out, and then discussed. Then the final conclusion is given in Sec. 9.

2 Elementary particles and there interactions within the standard model

Elementary particles are fundamental particles that are not composed of particles, they are the fundamental building block of matter. In the SM framework, subatomic particles are excitations of their respective fields. These excitations in the field then acquire their mass via interactions with the Higgs field, which is mediated by the Higgs boson. The current model of elementary particles includes quarks, leptons, and force particles. In the SM quarks and leptons are divided up into three generations, each including an up-type quark, a down-type quark, and two leptons, a charged lepton, and its associated neutrino. These subatomic particles interact via the strong, weak, electromagnetic, and gravitational force, each with its own force particles to mediate the interaction. The strong force only interacts with quarks, it is the force that binds quarks together to form other subatomic particles. The strong force is mediated by the gluon g which is a massless particle. The weak interaction is responsible for the interaction between subatomic particles that result in the decay of particles. It is mediated by the massive $W^{\pm}$ and Z bosons. The electromagnetic force and its mediator the photon γ is responsible for the interaction of charged particles. Gravity is the weakest of the fundamental forces and as such has a relatively small effect on subatomic particles. However, other than the other fundamental forces gravity does not balance out, allowing it to act upon large distances. This causes it to have a strong effect on the macroscopic scale. For example, gravity is responsible for all the large-scale structures currently present in the universe. [7] The gravitational force is postulated to be mediated by the Graviton but, as of writing this analysis, its existence has not yet been discovered.

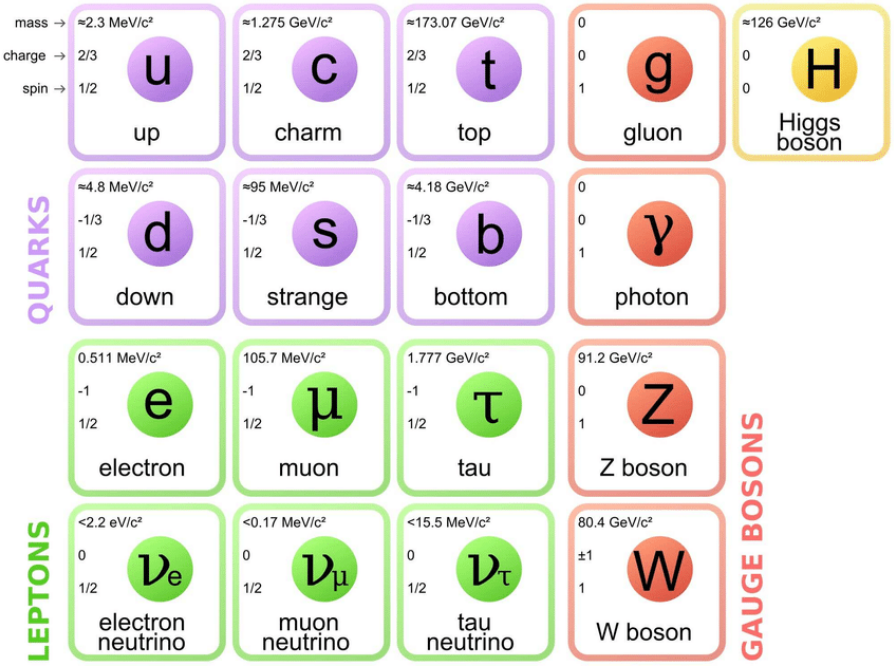

Figure 1: Fundamental particles of the SM. Figure acquired from [8].

2.1 Introduction $B_c^+ \to \tau^+ \nu_\tau$

LFU refers to symmetry where the electroweak coupling of leptons to gauge bosons where the coupling is independent of their flavour. [3] This excluded the Higgs field as the interaction with the Higgs field gives subatomic particles their mass. As the lepton mass differs between the different generations their interaction with the Higgs field also differs. As the LFU is dependent on the mass of the lepton, the exclusion of the Higgs field causes differences within LFU. Recent study of the transition $b \to c\ell^- \bar{\nu}_l$ in the $\mathcal{R}(D)$ and $\mathcal{R}(D^*)$, given in equation (2.1), show an enhanced ratio of 1.4σ and 2.8σ respectively,

when compared to the SM. [4]

$$\mathcal{R}(D^{(*)}) = \frac{\mathcal{BR}(\bar{B} \to D^{(*)}\tau^-\bar{\nu}_\tau)}{\mathcal{BR}(\bar{B} \to D^{(*)}\ell^-\bar{\nu}_l)}. \tag{2.1}$$

This deviation from the SM hint toward LFU violation and BSM. However, this can not yet be considered a new discovery as in particle physics something is considered a new discovery if the measurement deviates from the SM prediction with 5σ. [9]

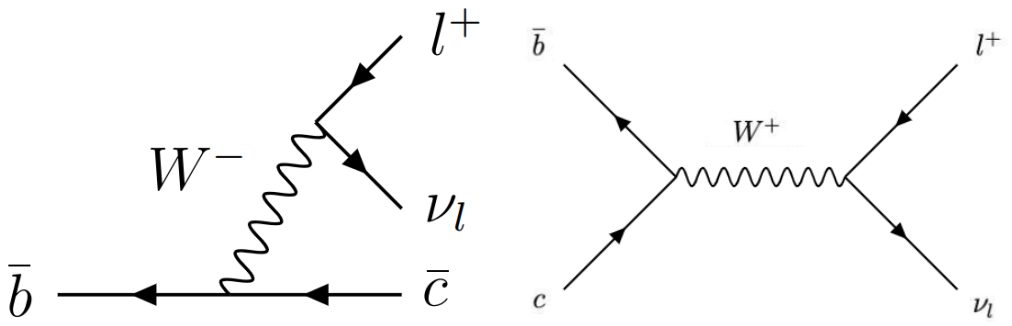

Figure 2: Feynman diagram of the $b \to c\ell^+\nu_l$ (left) $bc \to \ell^+\nu_l$ transition(right).

One transition that could give more inside into possible LFU violation is the transition of $\bar{b}c \to \ell^+\nu_l$ depicted in figure 2. The $\bar{b}c \to \ell^+\nu_l$ is on the quark-level identical to the $b \to c\ell^-\bar{\nu}_l$ transition as such it can give a different perspective on the results of the $b \to c\ell^-\bar{\nu}_l$ transition. The $\bar{b}c \to \ell^+\nu_l$ describes the decay of the $B_c^+ \to \tau^+\nu_\tau$ which has, as of this moment, no measured branching fraction. However, by use of the SM calculations done by Ref [10] predict for the B_c^+ decay the following branch fractions,

$$\mathcal{BR}(B_c^+ \to \tau^+\nu_\tau)^{SM} = (1.95 \pm 0.09) \times 10^{-2}. \tag{2.2}$$

And calculations by Ref [11] and Ref [12] predict the B_c^+ decay branch fraction to be,

$$\mathcal{BR}(B_c^+ \to \tau^+\nu_\tau)^{SM} = (2.25 \pm 0.21) \times 10^{-2}. \tag{2.3}$$

3 The Large Hadron Collider beauty

At the CERN the Large Hadron Collider (LHC) is located. One of the detectors in the LHC is the Large Hadron Collider beauty (LHCb), this detector is set up to study beauty quarks. An important aspect of this study CKM and CP violation, which can give information regarding the slight differences between matter and antimatter that is observed. The LHCb detector tests the SM and can as such be used to look for BSM. [13] Within the LHCb detector, two proton beams collide with a center of mass energy of $13 - 13.5TeV$. The LHCb is set up as a single-arm forward spectrometer, which makes use of the fact that the B hadrons are produced in the same forward cone. [14] The detector covers a pseudo-rapidity (η) range, given by equation (3.1), of $2 < \eta < 5$ which corresponding to a polar angle range of $0.77° < \theta < 15.4°$.

$$\eta = -\ln\left[\tan\left(\frac{\theta}{2}\right)\right]. \tag{3.1}$$

It is required from the LHCb detector that it is capable of both tracking and identifying particles, for this purpose the detector consist of a number of sub-detectors. The tracking system consists of the Vertex Locator (VELO) and the tracking stations; upstream tracker (UT), SciFi tracker, and muon detector. The Particle identification system consists of the two Ring Imaging Cherenkov Detectors; RICH1 and RICH2, The electromagnetic calorimeter, the hadronic calorimeter, and muon detector.

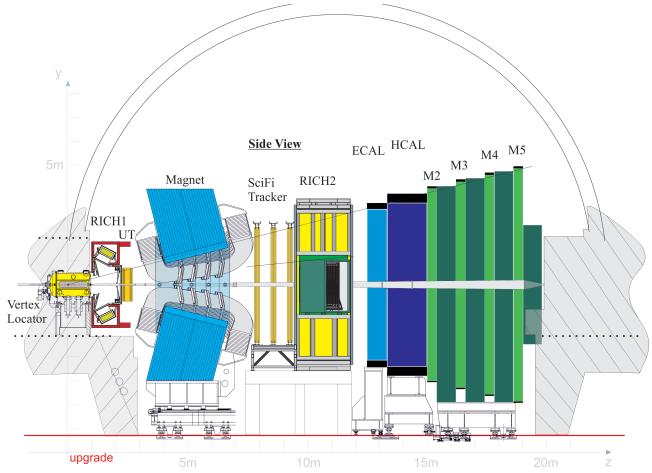

Figure 3: Visualization of the layout of the LHCb detector. Figure acquired from [15].

Within the LHCb detector, the VELO sub-detector is placed closest to the collision point. Its purpose is to determine the production and decay vertex of the signal particle with the goal of acquiring the coordinates of the track. Where, for example, the primary vertex (PV) in the LHCb depicts the location of the production of the B-meson, and the secondary vertex (SV) is the decay of produced B-meson. The detector consists of two retractible halves in which each halve contains 26 L-shaped silicon pixel detector modules, for a total of 52 modules, which are arranged as depicted in figure 4. Each half is enclosed in an aluminium box to shield the detector against radio-frequency picked from the beam, it further serves to separate the vacuum of the machine from the vacuum in which the modules are located. The retractable halves can place modules at a distance of 5.1mm from the beam axis and surround the interaction point. [16]

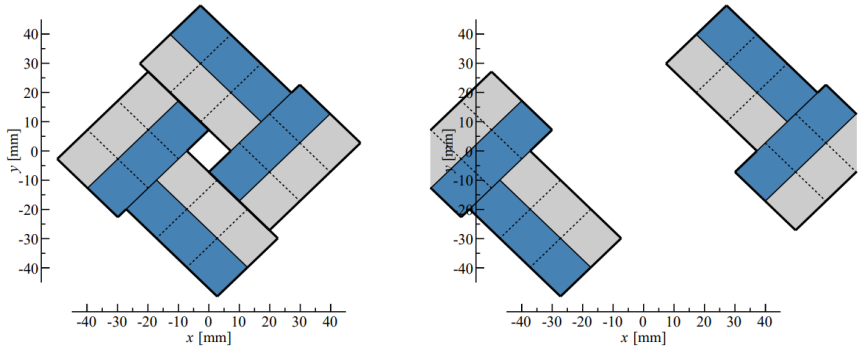

Figure 4: Visualization of the VELO with the modules open (left) and closed (right). Figure acquired from [16].

Together with the VELO detector the UT tracker and the SciFi tracker make up the tracking system in the LHCb detector. The tracking system is placed around the Dipole magnet, with the VELO and the UT tracker placed before the magnet and the SciFi tracker placed after the magnet. The magnet causes the charged particles to deflect. The amount of deflection is related to the particle's momentum. This allows the hits from the tracking system to give information regarding the charged particle's momentum.

To identify the charged hadrons over a wide momentum range the LHCb contains two Ring Imaging Chernekov detectors (RICH). The RICH1, placed after The VELO, is used for identifying charged particles with low momentum while the RICH2, placed after the SciFi tracking, identifies charge particles with high momentum. The RICH1 and RICH2, use the Cherenkov effect to identify particles. The Chernekov effect is the phenomenon where a charged particle that travels through a medium with a velocity higher than the speed of light in that medium emits radiation, which has been named Chernekov radiation. [17]

The electromagnetic calorimeter (ECAL) and the hadronic calorimeter (HCAL) measure the loss of energy of the particle as it travels through a layer. The calorimeters are located after the RICH2 detector, with the ECAL placed directly after the RICH2 followed by the HCAL. The ECAL is capable of measuring the energy of electromagnetically interacting particles, while the HCAL measures the energy composition of the hadrons. [18]

When a muon travels through the detector its momentum is measured by the tracking system, the muon stations are then used to identify muon candidates and match this information to a track provided by the tracking system. Within the LHCb the muon detector consisted of four rectangular shape moun stations (M2-M5) located behind the HCAL. The stations are interwoven with 80 cm thick iron absorption to select penetrating muons by filtering out low-energy particles. [18], [19]

4 The feasibility study

Within the preliminary results of the feasibility study, a framework was established in which the results were acquired. In order to be able to compare results, the same framework was used. This framework uses a multivariable analysis (MVA) (Sec.4.3) together with a monte carlo 2000 study (Sec.4.4) to acquire the results. For this purpose, the feasibility study considers a number of backgrounds (Sec.4.1) from which certain observables (Sec.4.2) were used.

4.1 Backgrounds

The feasibility study, on which this work is comparing to, determined the most dangerous backgrounds when trying to detect the $B_c^+ \to \tau^+\nu_\tau$. In this study, only backgrounds that include three pions were investigated. This approximation is allowed as other backgrounds could be suppressed using particle identification information from the RICH detectors, while the decay of charm hadrons to two or three hadrons are vetoed using mass vetoes. Furthermore, the contribution of the decays of charm hadrons to four hadrons is expected to not have a significant contribution.

The backgrounds that were considered were based on the work of [10]. From this study, it was determined that the decays that contain a heavy charged hadron which decays into a charged charmed hadron or τ, are considered the most dangerous background decays when trying to study $B_c^+ \to \tau^+\nu_\tau$.

As of writing this, the dangerous backgrounds are separated into two cocktails, D cocktail, and B cocktail. The decay included in each cocktail is discussed in Sec 4.1.1 and Sec. 4.1.2. Next to the decay in the D cocktail and B cocktail the $B^+ \to \tau^+\nu_\tau$ decay is also considered.

4.1.1 D cocktail

The D-cocktail, also referred to as charm cocktail, consists of the background decay where the parent particle is a D meson. They include,

- $D^+ \to \tau^+\nu_\tau$
- $D_s^+ \to \tau^+\nu_\tau$

4.1.2 B cocktail

B-cocktail consists of the background decay where the parent particle is a B meson. The B-cocktail consists of 7 decays, two of which directly decay into three pions while in all other decays the pions are created from the decay of the τ particle.

- $B^+ \to \bar{D}^0\tau^+\nu_\tau$
- $B^+ \to \bar{D}^{*0}\tau^+\nu_\tau$
- $B^+ \to \bar{D}^0\pi^+\pi^+\pi^-$
- $B^+ \to \bar{D}^{0*}\pi^+\pi^+\pi^-$
- $B^+ \to \bar{D}^0(D_s^+ \to \tau^+\nu_\tau)$
- $B^+ \to \bar{D}^{0*}(D_s^+ \to \tau^+\nu_\tau)$
- $B^+ \to \bar{D}^{0*}(D_s^{*+} \to \gamma(D_s^+ \to \tau^+\nu_\tau))$

4.2 The observables

The signal decay process $B_c^+ \to \tau^+\nu_\tau$, is divided into three vertexes; primary vertex (PV), secondary vertex (SV), and tertiary vertex (TV). Where the PV is the vertex in which the B_c^+ is created, the $B_c^+ \to \tau^+\nu_\tau$ decay vertex takes place at the SV, with the TV being the vertex in which the three pions are created. From this information different observables can be acquired, see figure 5. However, as the

LHCb detector can not measure the neutrinos no information regarding the SV can not be acquired, therefore identification of the decay relies on the reconstruction of the three pions, from which the TV can be determined. Making use of the information on the PV and TV the observables are determined.

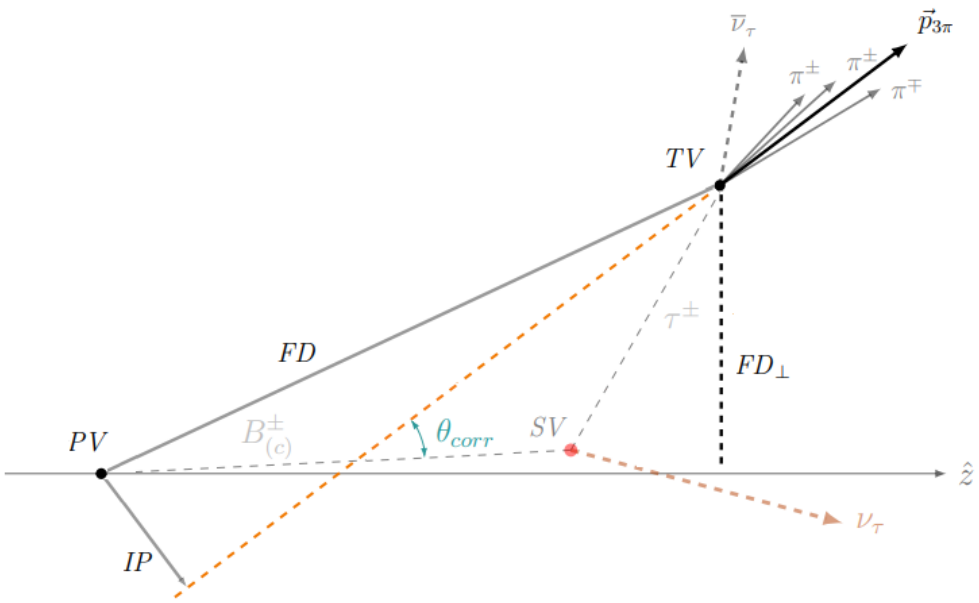

Figure 5: Depiction of the considered observables.

4.2.1 VELO hits

The VELO reconstructs the tracks of all charged particles, from these tracks the decay vertexes are determined. When a charged particle travels through a detector module it will leave a signal which is regarded as a hit. For the purpose of the analysis, the hits left by the three pions are not of interest but are however used in determining the decay vertex of the τ.

For selection, it is required that the events have at least one recorded hit of the parent particle, which for the $B_c^+ \to \tau^+\nu_\tau$ can be either from $B^+_{(c)}$ or τ^+. The location of the first hit (fh) is then determined and used to calculate the corrected mass as well as the missing mass (see Sec.4.2.2 and Sec. 4.2.3).

4.2.2 Corrected mass

As no information regarding the neutrino can be acquired, this information is lost. To retrieve some of this lost information the different variables are used. One such variable is the corrected mass given by,

$$m_{corr} = \sqrt{m_{3\pi}^2 + |\vec{p}_\perp(3\pi)|^2} + |\vec{p}_\perp(3\pi)| \tag{4.1}$$

Where $m_{3\pi}^2$ is given by,

$$m_{3\pi}^2 = \sqrt{E_{3\pi}^2 + \vec{p}_{3\pi}^2} \tag{4.2}$$

With $E_{3\pi}$ and $p_{3\pi}$, are the combined energy and momentum of the 3π-system respectively.

The $\vec{p}_\perp$ is the summation of the momentum of the three π particles, perpendicular to the flight direction of the B-meson. Where the flight direction is approximated by use of the location of the fh.

The corrected mass can be used to distinguish between signal and background as the $\vec{p}_\perp$ will differ depending on what other particles are produced in the considered event.

4.2.3 Missing mass

As has been stated not all particles can be detected, like the neutrino, to infer if there is an undetected particle that takes part in the event, the missing mass m^2_{miss} is used. The missing mass is defined by,

$$m^2_{miss} = (p^\mu_B - p^\mu_{3\pi})^2 = m^2_B + m^2_{3\pi} - 2p^\mu_B p^\mu_{3\pi} \tag{4.3}$$

where (p^μ_B) and $(p^\mu_{3\pi})$ are the four-momentum of the B-meson and three pions respectively. The m_B is the known mass of the B-meson and $m_{3\pi}$ is the invariant mass of the three pions.

The missing mass is reconstructed by measuring the momenta of the three pions and the position of the fh. If a deviation from the expected value of the missing mass is measured this can indicate the presence of additional undetected particles.

It should be noted that in the reconstruction of the missing mass, the following approximations need to be made.

- The unitary vector $\vec{u}_B$ in the B-meson flight direction is approximated as the direction from PV to the location of the fh
- $(p_B)_z = \left(\frac{m_{B_c^+}}{m_{3\pi}}\right)(p_{3\pi})_z$
- $p_B = \frac{(p_B)_z}{(u_B)_z}$
- $p^\mu_B = \begin{pmatrix} \sqrt{m^2_B + p^2_B} \\ p_B \vec{u}_B \end{pmatrix}$

4.2.4 Opening angle

The opening angle is the angle between the τ particle and the ν_τ that is produced in the decay of the $B^+_{(c)}$. As no information on the ν_τ is acquired from the detector this value can not be directly measured. As an alternative, the angle between the flight directions of the three pions and the direction of the PV to the fh is used. This experimentally measured angle is called θ_{corr}.

4.2.5 Impact parameter

The impact parameter (IP) is the distance between the point of closest approach of a particle's track and the defined primary vertex (PV) of the event to which the particle is associated. Because of this, the IP for a particle will differ depending an the manner in which it is created. This makes the IP value effective in differentiating particles that originate from the PV and those that form through intermediate particles.

4.2.6 Flight distance

The flight distance (FD) is the distance between the defined PV and TV. This distance will differ depending on the lifetime of the particles and can, as such, be used to distinguish between events that consider long (or short) lived particles.

Other than the FD the transverse flight distance ($FD_\perp$) is also considered. The $\text{FD}_\perp$ is the component of the flight distance that is perpendicular to the beam direction.

4.2.7 Momentum

The mass, the corrected mass, and the missing mass all depend on the momentum ($p_{3\pi}$) of the three pions or their transverse momentum ($p_\perp(3\pi)$). From this, it can easily be concluded that the momentum of the three pions contains important information regarding the decay channel and serves as an important observable within the analysis.

4.3 Multivariate Analysis

In this analysis, it is desired to accurately distinguish signal decays from background decays. For this purpose, the observables mentioned above are used to perform a multivariate analysis (MVA). The MVA is performed by use of the GradientBoostingClassifier (GBC) algorithm within the scikit-learn library. [20] For training the MVA with the GBC algorithm a $70 - 30$ split in the data is used, where 70% is used for training and 30% for testing.

4.3.1 Comparing the performance

To verify the performance of the MVA a test dataset is used. The purpose of this verification is to see if the MVA correctly labels the event as background or signal. For this purpose, the labels positive and negative are given to signal and background decays respectively. Resulting in the classification of the signal (background) event which correctly flagged by the MVA as a signal (background), to be called a true positive (true negative), while a background (signal) event flagged as a signal (background) event, by the MVA, to be called a false positive (false negative). With this classification, one can plot the true positive vs false positive from which the area under the curve (AUC) is acquired. The AUC shows the relative performance of the MVA. An AUC value of 1 constitutes a perfect classification for that particular dataset.

4.3.2 Overtraining

When working with decision trees it can occur that the model is trained too well on its train dataset, which leads to a phenomenon known as overtraining. This can result in a model that classifies events based on statistical fluctuations. Resulting in a model that will not perform as intended for any new dataset. [21]

Within the GBC algorithm, this problem is minimized by using a boosted decision tree. In this process each iteration, in which a decision tree is created, a larger weight is assigned to misclassified events, allowing the next iteration to focus on eliminating these misclassifications.

To further evaluate the performance of the MVA and check for overtraining a Kolmogorov-Smirnov (KS) test is performed for signal and background samples. The KS test is a statistical measure that determines the dissimilarity between two probability distributions. The KS test performed results in KS statistics and p-value. The KS statistic quantifies the distance between the distribution function of the sample and the distribution function resulting from the reference sample distribution. The p-value indicates whether the samples are drawn from similar distribution or not. [22] A p-value that is < 0.05 usually indicates that the samples are drawn from different distributions, while a high p-value > 0.05 indicates that the samples are drawn from similar distributions. As such for a p-value < 0.05 we can state with a high likelihood that our model contains overtraining.

4.4 MC 2000 study

To extract the signal yields a likelihood fit was performed. A probability density function (PDF) is constructed by the use of Python and the ROOT framework. This resulted in separate PDFs for: $B_c^+ \to \tau^+\nu_\tau$, $B^+ \to \tau^+\nu_\tau$, $B^+_{cocktail}$ and $D_{cocktail}$, which where then combined into a single PDF. This PDF was then used to perform a total of 2000 pseudo-experiments where pseudo-datasets are generated from the PDF and then fitted to the PDF model. Such experiments are referred to as MC 2000 study.

The number of events used in the final PDF are as followed,

- N($B_c^+ \to \tau^+\nu_\tau$) = 1065 = 0.02% of PDF
- N($B^+ \to \tau^+\nu_\tau$) = 18811 = 0.40% of PDF
- N($B^+_{cocktail}$) = 2955611 = 62.78% of PDF

- N($D_{cocktail}$) = 1732349 = 36.80% of PDF

The number of events is based on their respective yield.

5 Simulation framework

Within this work, the simulation framework consists of three separate MC libraries, RapidSim, EvtGen [23], and Tauola, linked together to get the desired results.

5.1 RapidSim

RapidSim is a time-efficient generator of events that is based on a phase space decay model, it allows one to generate millions of events within a few seconds. It generates large samples of decays with momentum spectra, invariant mass resolutions, and efficiency shapes. Its efficiency lies in the fact that it does not simulate the detector response, it instead gives close approximations to what can be obtained from such simulations. [6] In this work RapidSim is called upon to generate the given decay events. It is given a decay file in which to be generated decay is specified, along with a configuration file in which the setting and variables of interest are defined. Specifically for the decay of the τ particle RapidSim uses EvtGen as a middle-man to have the decay generated by the use of Tauola. RapidSim does this by writing a DEC file that contains info regarding the decay and other appropriate information like the libraries it must use to generate the decay and the decay channels considered.

Within the configuration file, it is defined that the parent particle is generated within a pseudo-rapidity range of $1 < \eta < 6$ and a momentum (p) ranging from $0 - 100 GeV/c$.

5.2 Tauola

The TAUOLA library is an MC generator that is specifically developed to describe the decay of the τ lepton. The library Tauola gives a final state acquired by considering neutrinos, resonant distribution for intermediate particles, and complete spin structure throughout the entire decay process. [24] To achieve this the MC libraries, like Tauola, calculate the hadronic current J^{μ} for a specific decay process that describes the symmetries of that decay. This requires the hadronic current to span eight-dimensional space. The original Tauola library simulated the τ decays by simulating all subprocesses first independently, after which their correlation is restored by means of rejection. In this model, three-pseudoscalar currents are constructed as a weighted sum of products of Breit-Wigner functions. This is done by having the MC start with calculating the masses in the τ rest frame. The mass is determined from a random numbers between 0 and 1. Following this, the weight W is calculated. As there is little interest in the weighted events they are rejected by means of the rejection weight. [24]

Currently, several millions of events per channel are collected, due to this the statistical error has been reaching 0.03%. To be able to make accurate comparisons between theory and data, parameterizations of hadronic currents that result from theoretical models must be controlled to a technical precision that is better than 0.03% in MC generators. [25]. For this reason, a number of currents have been developed, by different collaborations, that can be implemented within the Tauola library. As of this moment, the standard current found within the library are the CLEO current; developed by the CLEO collaboration, and the BaBar current; developed by the BaBar collaboration. Within this analysis, the τ decay is simulated by use of the BaBar tune in Tauola.

The CLEO current uses the Breit-Wigner resonance model fitted to the CLEO results, for $\tau \longrightarrow \pi^{-}\pi^{0}\pi^{0}\nu_{\tau}$. No conversion to the $\tau \longrightarrow \pi^{-}\pi^{+}\pi^{-}\nu_{\tau}$ is made, the model is applied "as is" to the $\tau \longrightarrow \pi^{-}\pi^{+}\pi^{-}\nu_{\tau}$ decay. The Tauola CLEO tune is the current default in Tauola. [26]

The BaBar tune is an upgrade of the MC generator of Tauola that uses the resonance chiral lagrangian theory results. The resulting hadronic current is fine-tuned to the BaBar results for the $\tau \longrightarrow \pi^{-}\pi^{+}\pi^{-}\nu_{\tau}$. [27]

For the three-scalar decay, both currents make use of the same basic formula, given in equation 5.1. The main distinction in their respective currents arises from their description of the complex scalar functions F_i which is fitted to the data. [26, 28]

$$J^{\mu} = N \{T^{\mu}_{\nu} [c_1 (p_2 - p_3)^{\nu} F_1 + c_2 (p_3 - p_1)^{\nu} F_2 + c_3 (p_1 - p_2)^{\nu} F_3] + c_4 q^{\mu} F_4 - \frac{i}{4\pi^2 F^2} c_5 \epsilon^{\mu}_{\cdot\nu\rho\sigma} p_1^{\nu} p_2^{\rho} p_3^{\sigma} F_5 \Big\} . \tag{5.1}$$

Where N is the normalization constant. $T_{\mu\nu}$ is the transverse projector given by, $T_{\mu\nu} = g_{\mu\nu} - Q_{\mu}Q_{\nu}/Q^2$, with $Q^{\mu} = (p_1 + p_2 + p_3)^{\mu}$ which denotes the momentum of the hadronic system and $g_{\mu\nu}$ which represents the metric tensor. The pions four-momenta are denoted as p_1, p_2 and p_3, which is respectively ordered $\pi^-\pi^-\pi^+$ for the three-prong channel and $\pi^0\pi^0\pi^-$ for the one-prong channel. q^{μ} is the transfer momentum. The $\epsilon^{\mu}_{\cdot\,\nu\rho\sigma}$ is the Levi-Civita symbol. The constants c_i are the Clebsch-Gordan coefficients, they are defined specifically for the particular hadronic current that is used. [28]

6 The resonance structure

The full decay mode generated by Tauola, including the resonance particle, is $B_c^+ \to (\tau^+ \to \bar{\nu}_\tau(a_1^+(1260) \to \pi^+(\rho^0 \to \pi^+\pi^-)))\nu_\tau$. As such it is to be expected that the mass of the 3 pions would peak at the mass of $a_1^+(1260)$, and the mass of the π^+_1 and π^-_0 would peak at the ρ^0. The mass plot of the 2π (figure 7a) and 3π (figure 7b) system with the mass of the ρ^0 and $a_1^+(1260)$ as defined in Tauola to be 0.77 ± 0.15(GeV) and 1.27 ± 0.67(GeV) respectively. It should, however, be noted that RapidSim distinguishes between the same particle by giving it a number, as this decay results in two π^+ particles it distinguishes the two pions by calling one π^+_0 and the other π^+_1, but as RapidSim sees the two π^+ as coming from the same decay vertex, it randomly chooses which particle is which. As such depicting the mass spectrum of the π^+_0 and π^-_0 would result in the same conclusion.

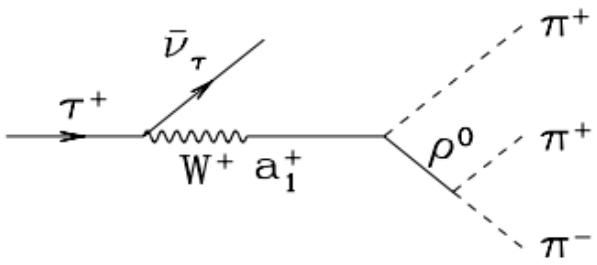

Figure 6: Decay of τ particle to three pions via its resonance particles. Acquired, but altered, from [29].

From figure 7a it can clearly be seen that the mass of the 2 pions, generated by Tauola, peaks at the mass of the ρ^0. For the 3π system due to the large uncertainty of the mass of the $a_1(1260)$ both the PHSP data as well as the data generated by Tauola fall within the accepted range for the $a_1(1260)$ particle and as both peaks are roughly the same distance from the $a_1(1260)$ defined mass of 1.27499998 GeV neither can be confidently linked to the $a_1(1260)$ particle. However, figure 7b shows no violations for the 3π system generated by Tauola and as such, taking into consideration the behavior depicted in figure 7a, it can be confidently stated that the decay mode is correctly generated by Tauola.

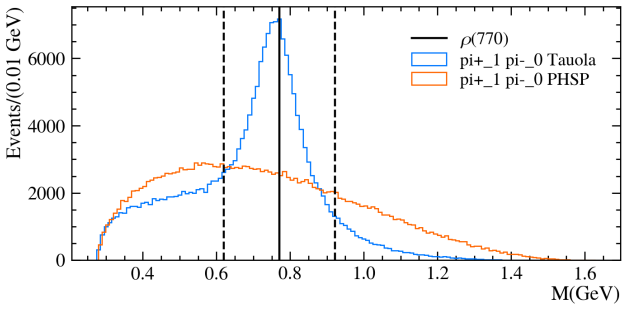

(a) 2π system

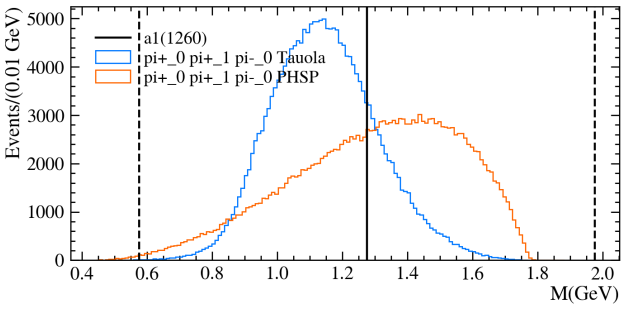

(b) 3π system

Figure 7: Plot depicting mass of the 2π system(left) and the 3π system(right) for the B_c^+ decay resulting MC simulation using PHSP and Tauola.

One of the manners in which we distinguish decays is via their corrected mass, as the introduction of the resonance structure within the decay alters the mass spectrum, logically it also alters its corrected mass spectrum. Comparison of the fh corrected mass spectrum for the decay generated by PHSP and by Tauola is depicted in figure 8. The figure shows a higher peak shifted slightly to a lower energy for the decay generated by Tauola.

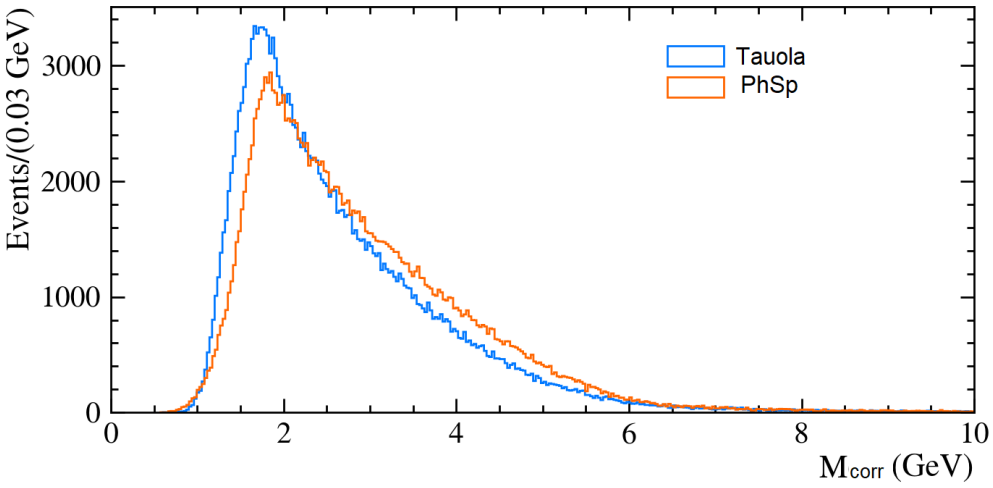

Figure 8: Corrected mass determined from first hit (fh) for $B_c^+ \to \tau^+\nu_\tau$.

6.1 Effect resonance structure on the other observables

The effect of the resonance structure of the τ particle for the observables listed in Sec. 4.2, shown in figure 9, shows no strong deviation. This is to be expected as the resonance particles are short-lived and will therefore not significantly affect the observables other than the mass spectrum. However, for all observables that are shown in figure 9, the resonance structure causes a slightly higher peak indicating a slightly higher localization of events is introduced by the resonance structure.

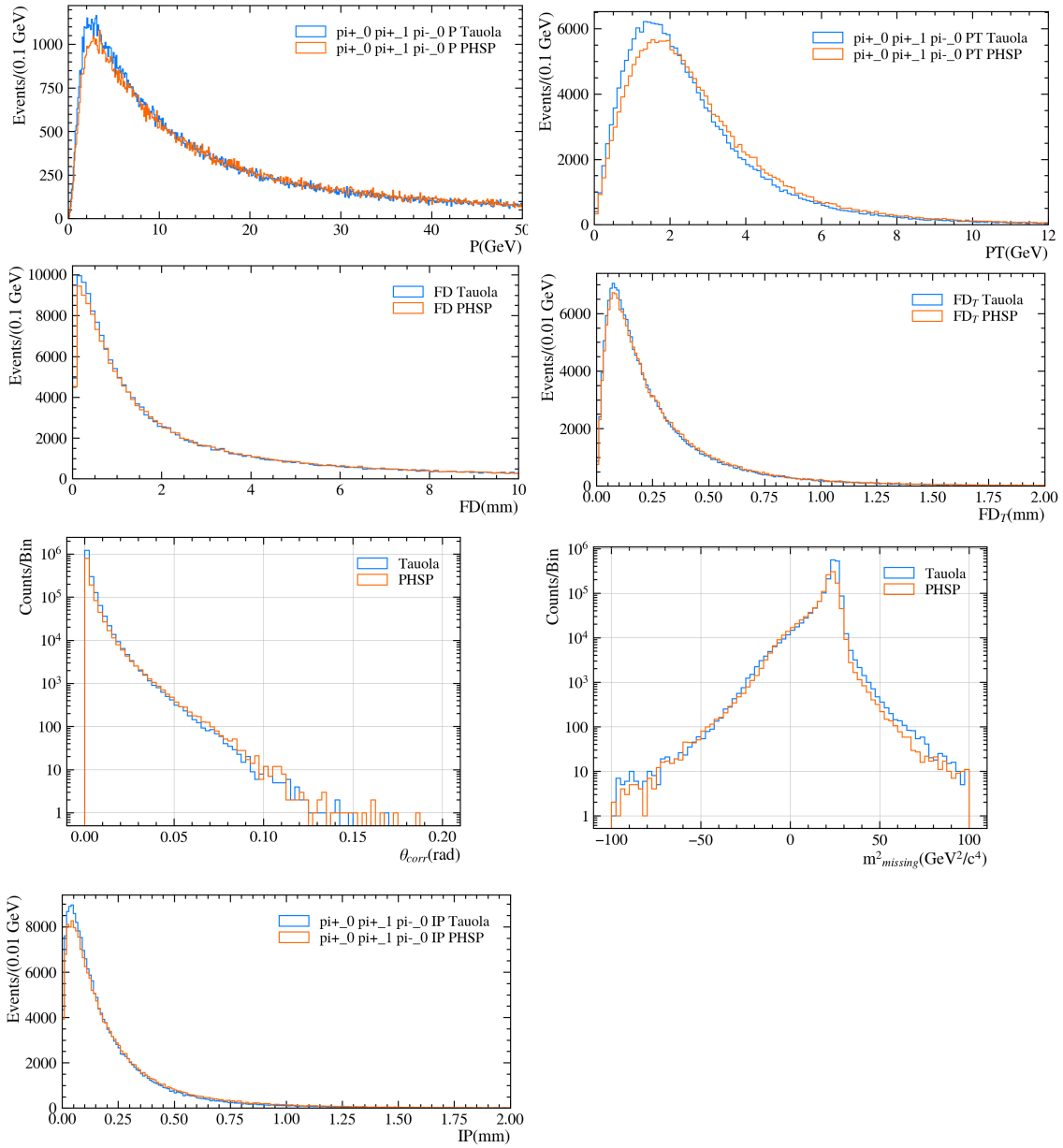

Figure 9: Comparison of observabels for PHSP data and data including τ resonance structure for the decay $B_c^+ \to \tau^+ \nu_\tau$.

7 Effect of the Resonance structure on the original MVA

To see the effect of the resonance structure, introduced by Tauola, on the performance of the original MVA which was trained on PHSP data, this MVA is used to fit the Resonance data.

Decay	Yield	Weight in MVA	Events in training	Events in testing
PHSP data				
$B_c^+ \to \tau^+\nu_\tau$	1065	50%	841722	360738
$B^+_{cocktail}$	2955611	$\simeq 31.5\%$	530679	227433
$D_{cocktail}$	17322349	$\simeq 18.5\%$	311042	133304
Resonance data				
$B_c^+ \to \tau^+\nu_\tau$	1065	50%	1267604	543259
$B^+_{cocktail}$	2955611	$\simeq 31.5\%$	799184	342507
$D_{cocktail}$	17322349	$\simeq 18.5\%$	468419	200751

Table 1: Amount of events used for the MVA.

The original MVA was trained with $B_c^+ \to \tau^+\nu_\tau$ as signal events and $D_{cocktail}$ and $B^+_{cocktail}$ decays as background events. The MVA was trained using a $50-50$ split where 50% of the total events were reserved for the signal decay events, $B_c^+ \to \tau^+\nu_\tau$, and 50% for events of the $D_{cocktail}$ and $B^+_{cocktail}$ decays, where their respective contribution was based on their expected yields. In table 1 the number of events for PHSP data, on which the original MVA is trained, and the resonance data show for training and testing. For the resonance data, the training events are not used within this section.

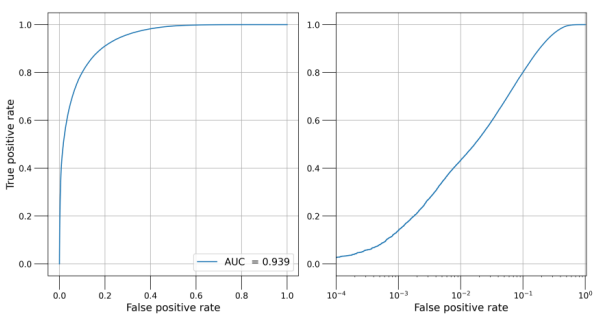

(a) AUC results using PHSP data

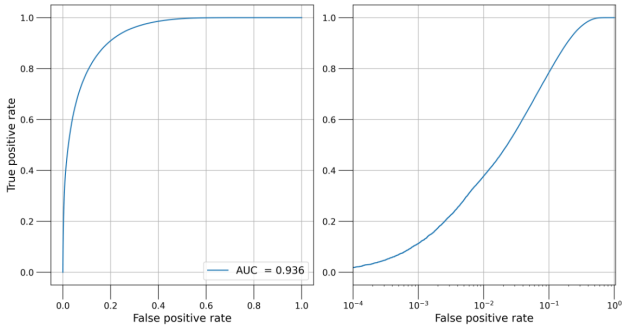

(b) AUC results using data with resonance structure

Figure 10: Plot depicting true positive rate vs false positive rate resulting from the MVA.

Within figure 10, the AUC resulting from the original MVA is depicted for PHSP data and data that includes the resonance structure of the τ particle. Appling the original MVA to data that includes the resonance structure of the τ particle results in an AUC value of 0.936 compared to an AUC of 0.939 for PHSP data. This result shows only a slight decrease in the MVA's capability to classify data that includes the τ resonance structure. A difference within the resulting AUC value, although it has been shown not to be a significant difference, is to be expected as the original MVA is trained to distinguish PHSP data. The impact of this difference in the AUC source is most noticeable when looking at the right panel of 10a and 10b. These figure shows the false positive rate, plotted on a logarithmic scale, vs the true positive rate. Around the false positive rate of 10^{-2} the figure shows a decrease in the true positive rate, indicating a lower fraction of signal to background in the events that the MVA classifies as signal.

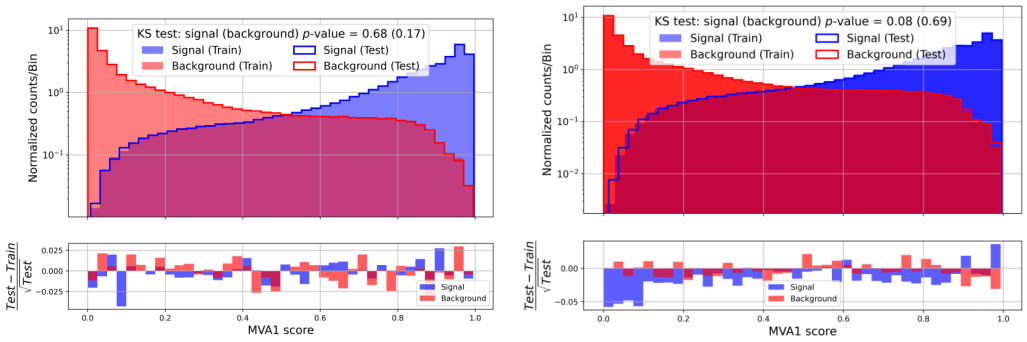

(a) Original **(b)** Test data is data with τ resonance structure

Figure 11: Figure depicting the results of the KS test. On the left side, the KS test for the original MVA is depicted where both train and test data is PHSP data, while on the right the resulting KS test is depicted where the test data is switched for data that included the τ resonance structure.

The result for the KS test are depicted in figure 11, where figure 11a depicts the KS test where both test and train data is PHSP data while in figure 11b the test data is data that includes the τ resonance structure. Comparing figure 11a and figure 11b p-value, it can be seen that the p-value for the signal decay decreases from 0.68 to 0.08, when switching the test data from PHSP data to data with the resonance structure, while for background this switch results in an increase of the p-value from 0.17 to 0.69. The decrease in the p-value for the signal decay is to be expected as the resonance structure changes the distribution of the decay making them less similar. This would also be expected for the p-value for the background decay, however, the results of the KS test show an increase. This effect is most likely associated with the presence of the $B^+ \to \bar{D}^0\pi^+\pi^+\pi^-$ and $B^+ \to \bar{D}^{0*}\pi^+\pi^+\pi^-$ decays within the background, as these decays have the most dominant contribution to the background events and are the only two decays considered that do not include a τ particle. A strong conclusion regarding this can however not be made without a more detailed study.

The most interesting thing to note from figure 11 is that for both signal and background the p-value in figure 11b is > 0.05. This indicates that the original MVA is not inefficient in characterize data that includes the τ resonance structure.

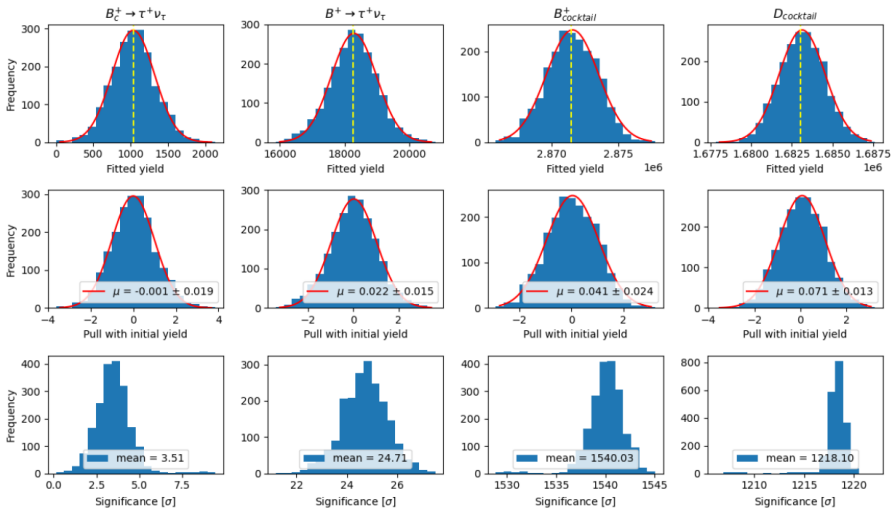

Figure 12: MC 2000 study resulting from the original MVA with PHSP data.

7.1 MC 2000 study

The result for the MC 2000 study is depicted in figure 12 and figure 13, for PHSP data and data with resonance structure respectively. These figures show 4 columns where each column represents the result for each component of the PDF. The first row depicts the distribution of the fitted yields, these results are fitted with a Gaussian function to acquire the mean (μ_{yield}) and standard deviation (σ_{yield}). These values are then used to acquire the results depicted in the second row that displays the pull of the distribution, which is the difference between the mean μ_{yield} and the true yield divided by σ_{yield}. Within the third row, the significance of the components is depicted. The significance is calculated by dividing μ_{yield} by σ_{yield}.

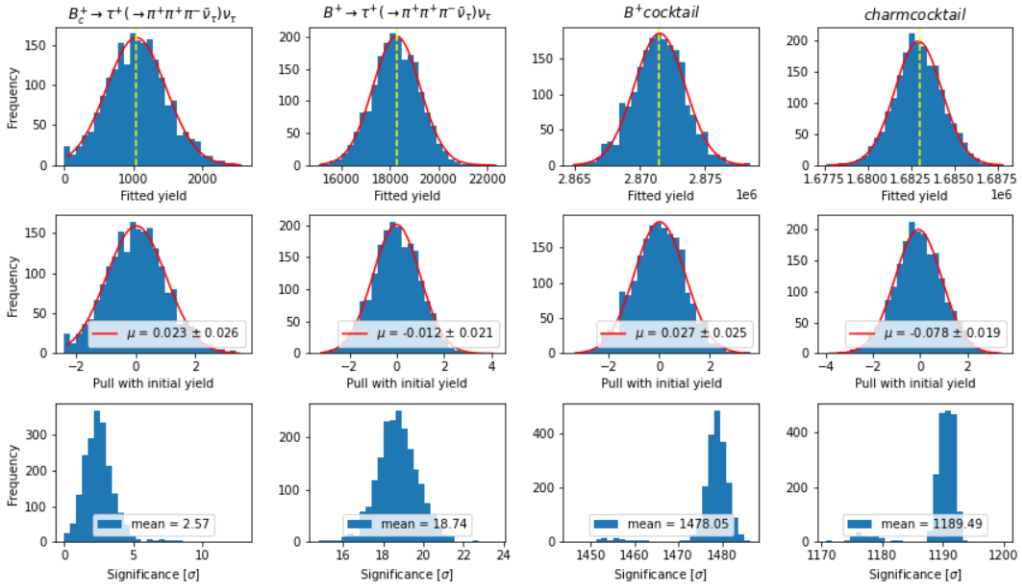

Figure 13: MC 2000 study resulting from the original MVA with data that includes the τ resonance structure.

The importance of the pull in figure 12 and figure 13, is confirmation of the correctness of the result. For both figures the pull of the components is closely around the value zero, this indicated an agreement with the fitted yield and true yield and shows that the method used can be considered reliable. Comparing the significance, the inclusion of the resonance structure shows a decrease in the significance for all considered components. The most significant decrease is that of 1σ in the signal decay. As the significance is required to be equal or above 5σ before it can be confidently stated that decay is observed, these results show that the inclusion of the resonance structure requires further development of the current method before it can distinguish the signal decay within real data.

7.2 MVA trained on data with resonance structure

The deviation in significance is to be expected as the original MVA is trained on PHSP data and will therefore be optimized to distinguish PHSP decays. To get a better inside into the MVA's capability of distinguishing decays when the resonance structure of the τ particle is taken into account, it is logical to look at an MVA that is trained on data that includes the resonance structure. This MVA will be referred to as MVA2.

The resulting AUC and KS test for MVA2 is depicted in figure 14a and 14b respectively. It is of interest to note that while the original MVA consisted of 200 stages, in which each stage leads to a decision tree, for MVA2 the same number of stages resulted in a p-value of 0.04 for the signal decay. As this indicates overtraining, MVA2 is trained with a lower number of stages, namely 150 stages. MVA2 resulted in an AUC of 0.934 which is a small decrease of 0.002 in comparison with the AUC of the original MVA when fitting data that includes the resonance structure.

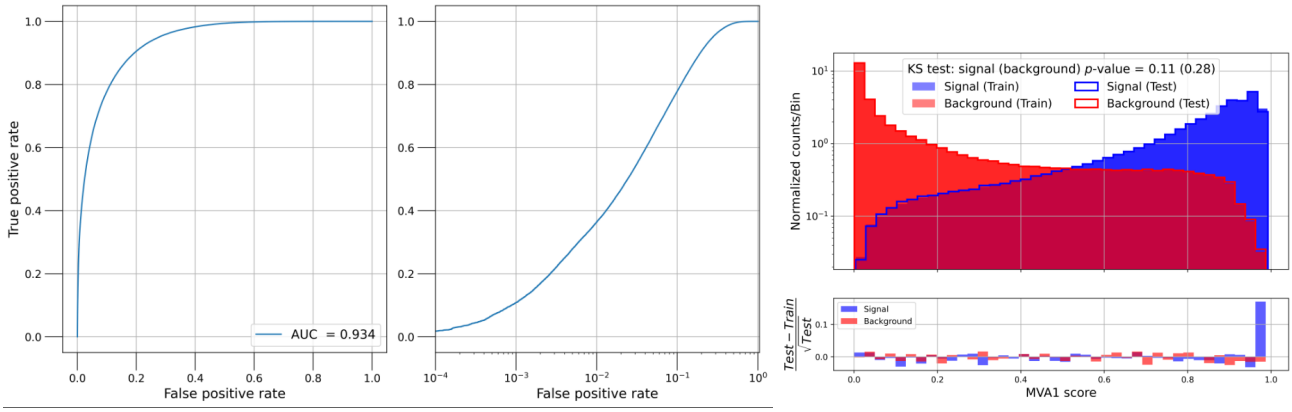

(a) ROC **(b)** KS test

Figure 14: Figure depicting ROC (left) and KS test (right) for MVA2.

Performing again the 2000 MC study, depicted in figure 15, it shows negligible differences in the resulting significance compared to results shown in figure 13. This indicates that with the current observables an MVA trained on PHSP data gives similar results when fitting data that includes the resonance structure of the τ particle, as an MVA that is trained with that data.

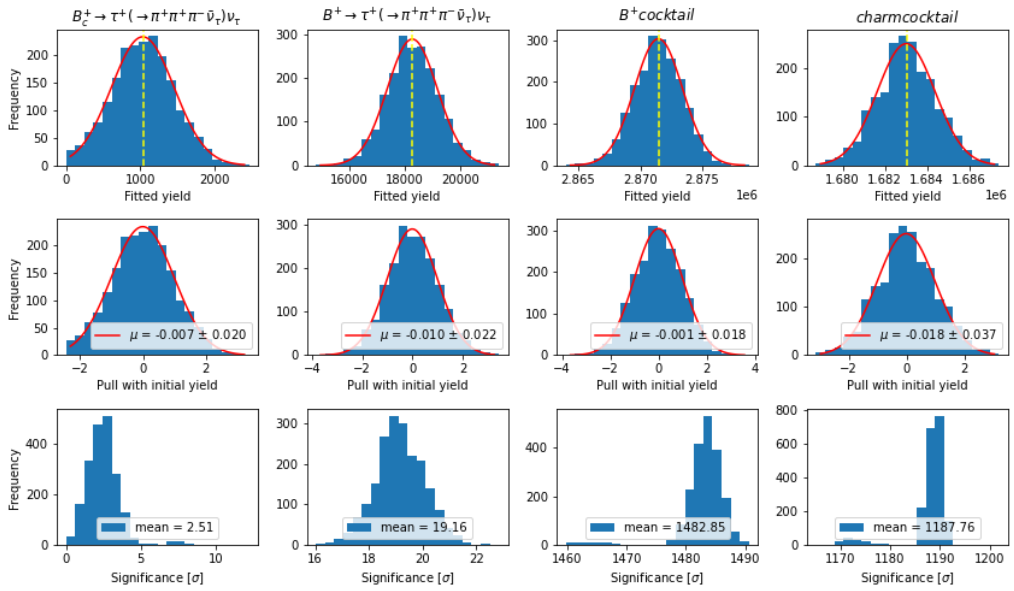

Figure 15: Resutls of 2000 MC study for MVA trained with data that includes resonance structure.

8 Including the mass of the 3 pions as observable

As shown in Sec.6 the introduction of the resonance structure has the largest effect on the mass spectrum of the three pions. However, in the original MVA, the mass of the three pions is not taken as observable. The choice not to use the mass of the three pions as observable is justified as the results of an MVA trained on PHSP data, using the mass of the three pions as observable next to the other aforementioned observables, results in a negligible difference in the resulting significance, see appendix B. This suggests that the mass of the three pions is strongly associated with another observable within the original MVA and could therefore be omitted. As now the resonance structure of the τ particle is taken into consideration this creates a strong distinction between the decays that contains a τ particle and the two that do not, namely $B^+ \to \bar{D}^0\pi^+\pi^+\pi^-$ and $B^+ \to \bar{D}^{0*}\pi^+\pi^+\pi^-$. As the $B^+ \to \bar{D}^0\pi^+\pi^+\pi^-$ and $B^+ \to \bar{D}^{0*}\pi^+\pi^+\pi^-$ decays have the largest branching fraction of all considered decays, this distinction allows separation of a large fraction of events.

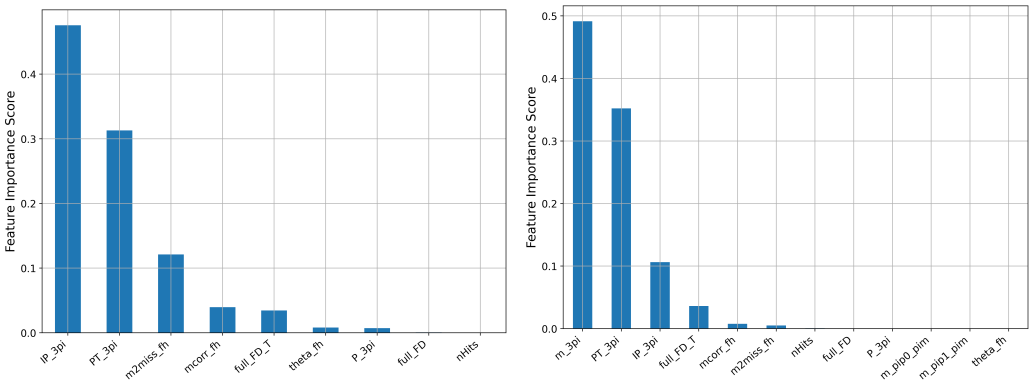

(a) MVA original **(b)** All observables

Figure 16: Observable importance score of the observables by which the MVA is trained.

As shown in figure 16, when including the mass of the three pions it becomes the most important feature for the MVA. This also becomes visible in the increase in the significance of the signal decay, shown in figure 17. However, as the inclusion of the τ resonance state improves the description of the considered decay that includes a τ particle, for completeness, the description of the remaining decays should also be improved.

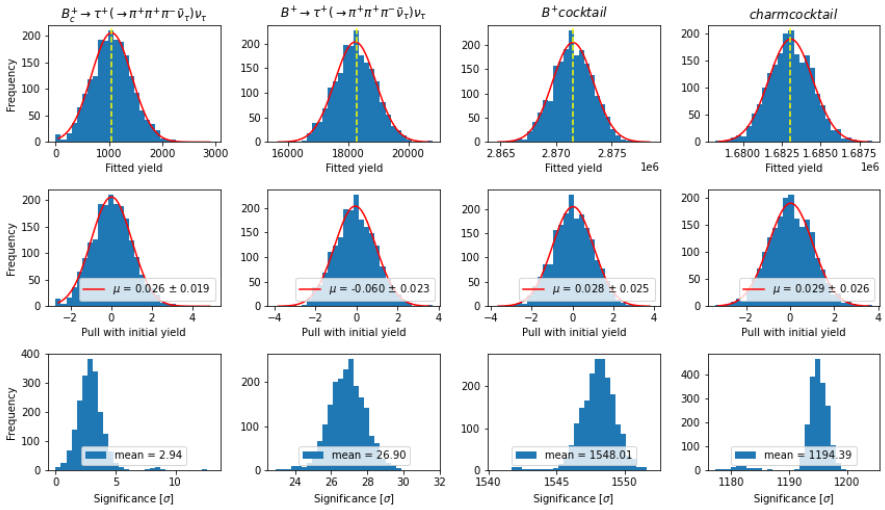

Figure 17: Results of MC 2000 study of MVA that includes all observables.

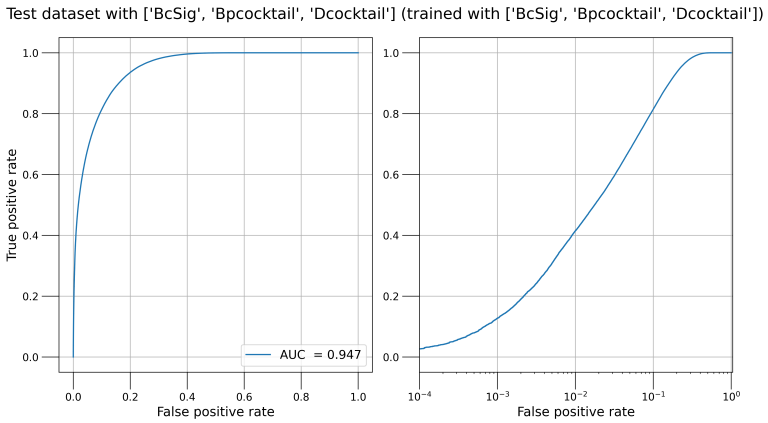

Figure 18: True positive rate Vs false positive rate, resulting from MVA trained on all observables.

8.1 Description of the direct decays

As stated above, the introduction of the τ resonance state requires that the description of the two remaining decays, which do not include the τ particle, also be improved to paint a more complete picture. This refers to the $B^+ \to \bar{D}^0\pi^+\pi^+\pi^-$ and $B^+ \to \bar{D}^{0*}\pi^+\pi^+\pi^-$ decays. A more complete description of those decays is of importance as the $B^+ \to \bar{D}^0\pi^+\pi^+\pi^-$ and $B^+ \to \bar{D}^{0*}\pi^+\pi^+\pi^-$ decay make up the largest fraction in the total number of events used in the analysis. As these decays do not include the resonance structure of the τ particle the MVA can easily distinguish them. Furthermore, as the more complete description will show, the decay channels of the $B^+ \to \bar{D}^0\pi^+\pi^+\pi^-$ and $B^+ \to \bar{D}^{0*}\pi^+\pi^+\pi^-$ decay also include the $a_1(1260)$ and ρ^0 particle.

Decay channel	Branch fraction	Label
$B^+ \to (\bar{D}^0 \to K^+\pi^-)(a_1(1260) \to (\rho^0 \to \pi^+\pi^-)\pi^+)$	0.66	A.0
$B^+ \to (\bar{D}^0 \to K^+\pi^-)(\rho^0 \to \pi^+\pi^-)\pi^+$	0.08	A.1
$B^+ \to (\bar{D}^0 \to K^+\pi^-)(f2 \to \pi^+\pi^-)\pi^+$	0.12	A.2
$B^+ \to (\bar{D}_{10} \to (D^{*+} \to (D^0 \to K^+\pi^-)\pi^+)\pi^-)\pi^+$	0.098	A.3
$B^+ \to (\bar{D}_{10} \to (D^0 \to K^+\pi^-)\pi^-\pi^+)\pi^+$	0.042	A.4

Table 2: Different decay channels for the $B^+ \to \bar{D}^0\pi^+\pi^+\pi^-$ decay.

In table 2, 3 and 4 the improved description of the $B^+ \to \bar{D}^0\pi^+\pi^+\pi^-$ and $B^+ \to \bar{D}^{0*}\pi^+\pi^+\pi^-$ decays are shown. Table 2 shows the decay channels with their respective branch fraction for the $B^+ \to \bar{D}^0\pi^+\pi^+\pi^-$ decay. In table 3 and table 4 two discription of the $B^+ \to \bar{D}^{0*}\pi^+\pi^+\pi^-$ decay are shown. They differ in their description of the $\bar{D}^{0*}$ decay, where table 3 shows the $\bar{D}^{0*}$ decay directly to a γ particle and table 4 shows the decay of $\bar{D}^{0*}$ to two γ particles via a π^0, for convenience these descriptions will be referred to as gamma 1 and gamma 2 respectively. The two distinct descriptions of the $B^+ \to \bar{D}^{0*}\pi^+\pi^+\pi^-$ decay are considered separately in order to visualize its individual effect and draw a conclusion on the manner in which these descriptions need to be included in a future analysis.

Decay channel	Branch fraction	Label
$B^+ \to (\bar{D}^{0*} \to (D^0 \to K^+\pi^-)\gamma)(a_1(1260) \to (\rho^0 \to \pi^+\pi^-)\pi^+)$	0.70	B.0
$B^+ \to (\bar{D}^{0*} \to (D^0 \to K^+\pi^-)\gamma)(f2 \to \pi^+\pi^-)\pi^+$	0.13	B.1
$B^+ \to (\bar{D}^{0*} \to (D^0 \to K^+\pi^-)\gamma)(\rho^0 \to \pi^+\pi^-)\pi^+$	0.12	B.2
$B^+ \to (\bar{D}^{0*} \to (D^0 \to K^+\pi^-)\gamma)\pi^+\pi^+\pi^-$	0.05	B.3

Table 3: Description of decay channels of $B^+ \to \bar{D}^{0*}\pi^+\pi^+\pi^-$ decay that result in one γ in final state (gamma 1).

Decay channel	Branch fraction	Label
$B^+ \to (\bar{D}^{0*} \to (D^0 \to K^+\pi^-)(\pi^0 \to \gamma\gamma))(a_1(1260) \to (\rho^0 \to \pi^+\pi^-)\pi^+)$	0.70	C.0
$B^+ \to (\bar{D}^{0*} \to (D^0 \to K^+\pi^-)(\pi^0 \to \gamma\gamma))(f2 \to \pi^+\pi^-)\pi^+$	0.13	C.1
$B^+ \to (\bar{D}^{0*} \to (D^0 \to K^+\pi^-)(\pi^0 \to \gamma\gamma))(\rho^0 \to \pi^+\pi^-)\pi^+$	0.12	C.2
$B^+ \to (\bar{D}^{0*} \to (D^0 \to K^+\pi^-)(\pi^0 \to \gamma\gamma))\pi^+\pi^+\pi^-$	0.05	C.3

Table 4: Description of decay channels of $B^+ \to \bar{D}^{0*}\pi^+\pi^+\pi^-$ decay that result in two γ in final state (gamma 2).

8.2 Simulation of decay

Generation of events for the new descriptions of the $B^+ \to \bar{D}^0\pi^+\pi^+\pi^-$ and $B^+ \to \bar{D}^{0*}\pi^+\pi^+\pi^-$ decays is done through the use of EvtGen. To achieve the link setup between RapidSim and Evtgen is used, but as this decay does not include a τ particle EvtGen performs the job itself other than sending it to the Tauola library.

8.3 Effect on the mass spectrum

As shown in figure 16b the most important observable for the MVA was the mass of the three pions. As such the largest effect on the resulting significance will result from the change in the mass spectrum of the three pions. The mass spectrum of the improved descriptions, for the $B^+ \to \bar{D}^0\pi^+\pi^+\pi^-$ and $B^+ \to \bar{D}^{0*}\pi^+\pi^+\pi^-$ decays, is shown in figure 19, where, for comparison, the original mass spectrum of the aforementioned decays is also shown.

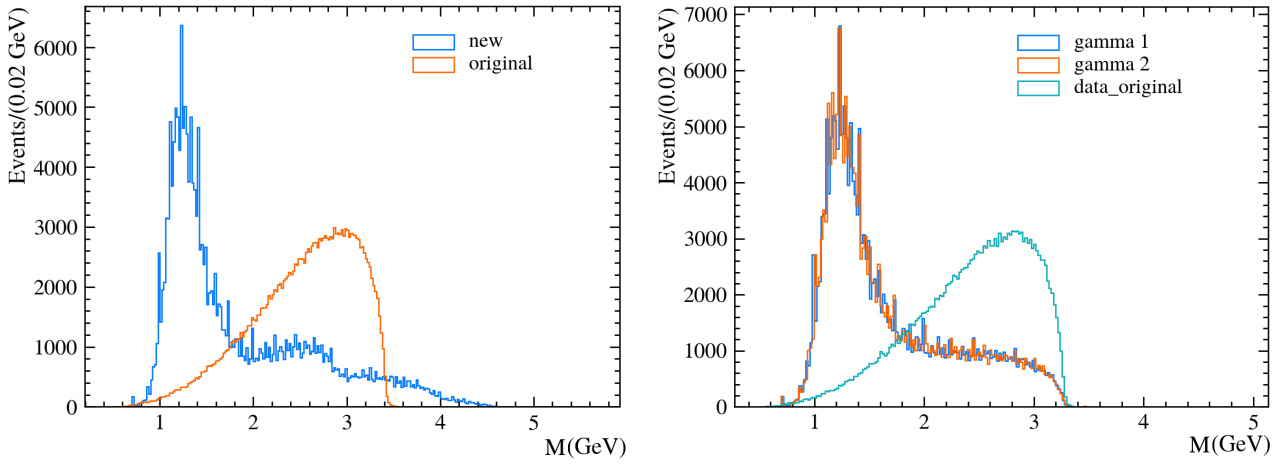

(a) $B^+ \to \bar{D}^0\pi^+\pi^+\pi^-$ **(b)** $B^+ \to \bar{D}^{0*}\pi^+\pi^+\pi^-$

Figure 19: Three pion mass spectrum.

The most important structure introduced by the new description of the $B^+ \to \bar{D}^0\pi^+\pi^+\pi^-$ and $B^+ \to \bar{D}^{0*}\pi^+\pi^+\pi^-$ decays, as can be seen in figure 19, is the strong peak that lies within the 0.8 to 1.8 GeV range, present in both decays. The presence of this peak is of importance as roughly within the same range as the mass spectrum for the three pions of the $B_c^+ \to \tau^+\nu_\tau$ peaks. From figure 20 it can be seen that this peak arises from the dominant decay channel in both decays, namely the decay channel with a branch fraction of 0.66 and 0.70 for $B^+ \to \bar{D}^0\pi^+\pi^+\pi^-$ and $B^+ \to \bar{D}^{0*}\pi^+\pi^+\pi^-$ respectively. As the three pions in these decay channels originate from the a_1 particle which decays equivalent to the a_1 particle in the τ decay, this similarity confirms the importance of the improved description of the $B^+ \to \bar{D}^0\pi^+\pi^+\pi^-$ and $B^+ \to \bar{D}^{0*}\pi^+\pi^+\pi^-$ decays.

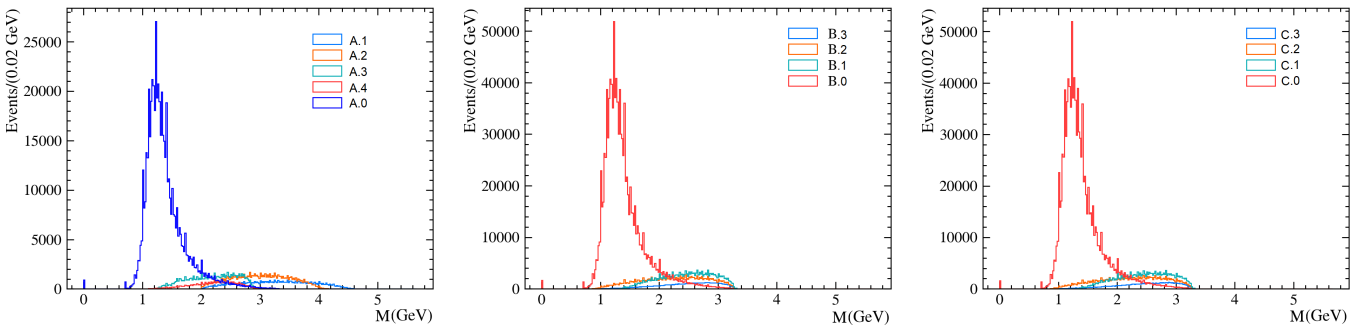

(a) $B^+ \to \bar{D}^0\pi^+\pi^+\pi^-$ **(b)** Gamma 1 **(c)** Gamma 2

Figure 20: Contribution of each branch fraction to the three pion mass spectrum, labeled as shown in table 2, 3 and 4.

For the two new descriptions for the $B^+ \to \bar{D}^{0*}\pi^+\pi^+\pi^-$ decay, shown in figure 19b, it can be seen that the mass spectrum of the three pions results in a negligible difference between the gamma 1 and

gamma 2 descriptions. This observation seems to hint towards a small to negligible effect the different descriptions will have on the significance resulting from this analysis.

8.4 Effect on the other observables

The effect of the new description for the $B^+ \to \bar{D}^0\pi^+\pi^+\pi^-$ and $B^+ \to \bar{D}^{0*}\pi^+\pi^+\pi^-$ decays, has on the observables, without the mass of the three pions, is shown in figure 22 and figure 21 respectively. Most notable within these figures is the similar distribution of the gamma 1 and gamma 2 descriptions for the observables.

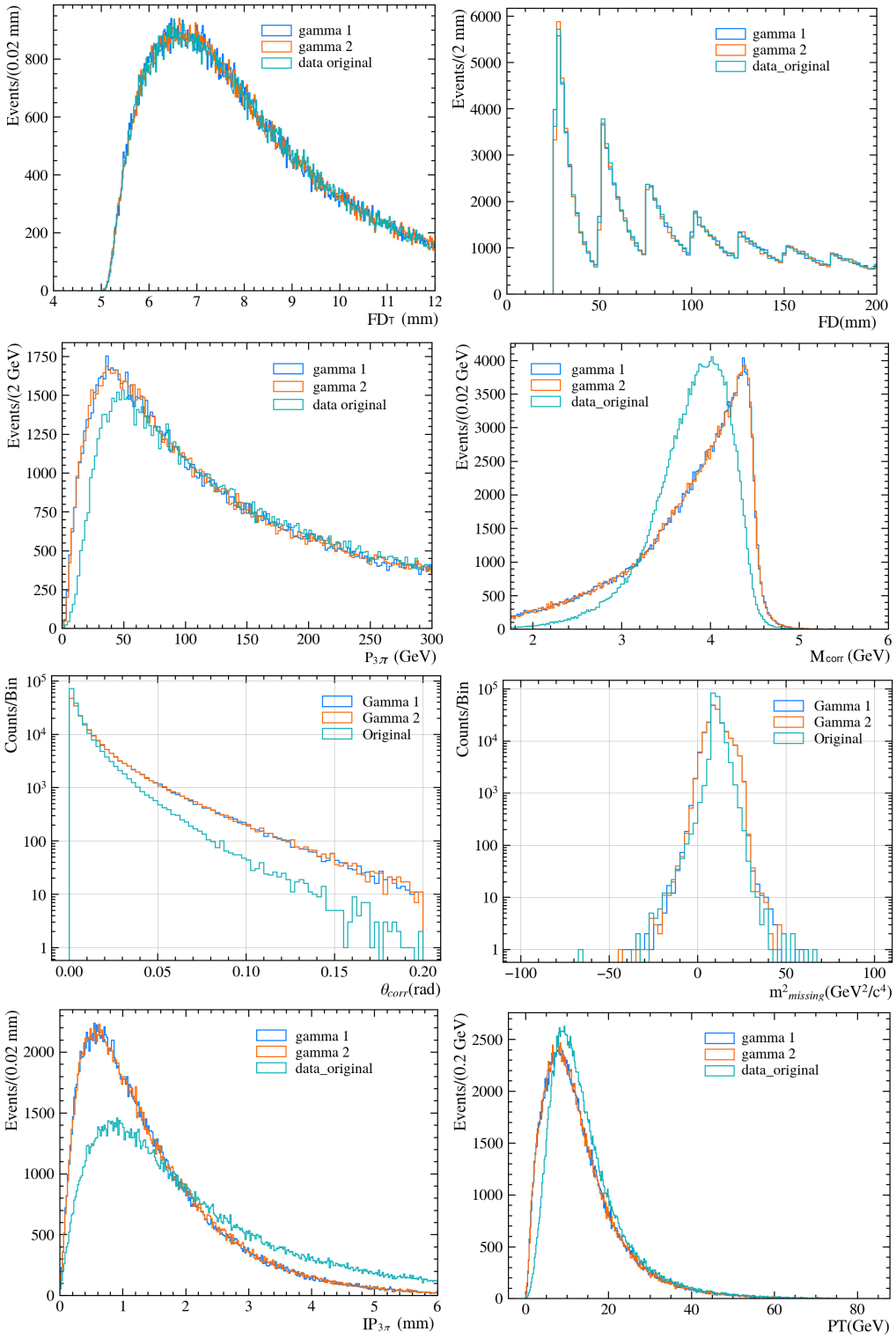

Figure 21: Comparison the observables of $B^+ \to \bar{D}^{0*}\pi^+\pi^+\pi^-$ descriptions.

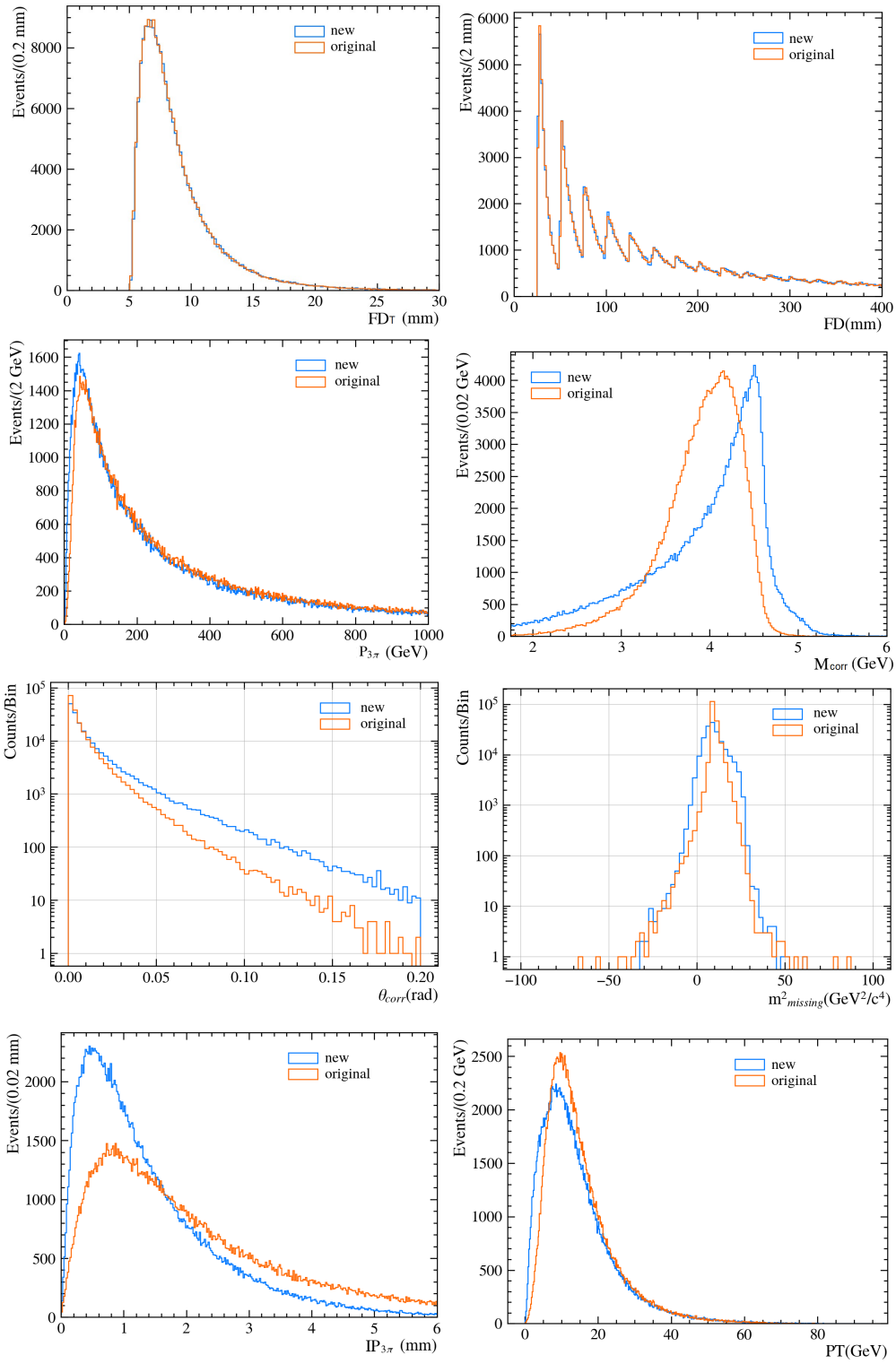

Figure 22: Comparison the observables of $B^+ \to \bar{D}^0\pi^+\pi^+\pi^-$ descriptions.

8.5 Effect on the MVA

As mentioned, the gamma 1 and gamma 2 description are considered separately, resulting in two MVAs. The two MVAs are named MVA gamma 1 and MVA gamma 2 for the gamma 1 and gamma 2 descriptions respectively. From these two MVAs the importance score of the used variables, shown in figure 23, is again acquired. This figure shows that the mass of the three pions is no longer the most important observable by which it makes distinctions. This shows that the MVA no longer makes as strong of a distinction between the decays that contain the τ resonance structure and those that do not. While the mass of π^+ and π^- combination are taken into account in the result of figure 17, MVA gamma 1 and MVA gamma 2 are not trained with those observables. This decision was made due to the additional complications it introduced as well as its zero importance score in figure 16b.

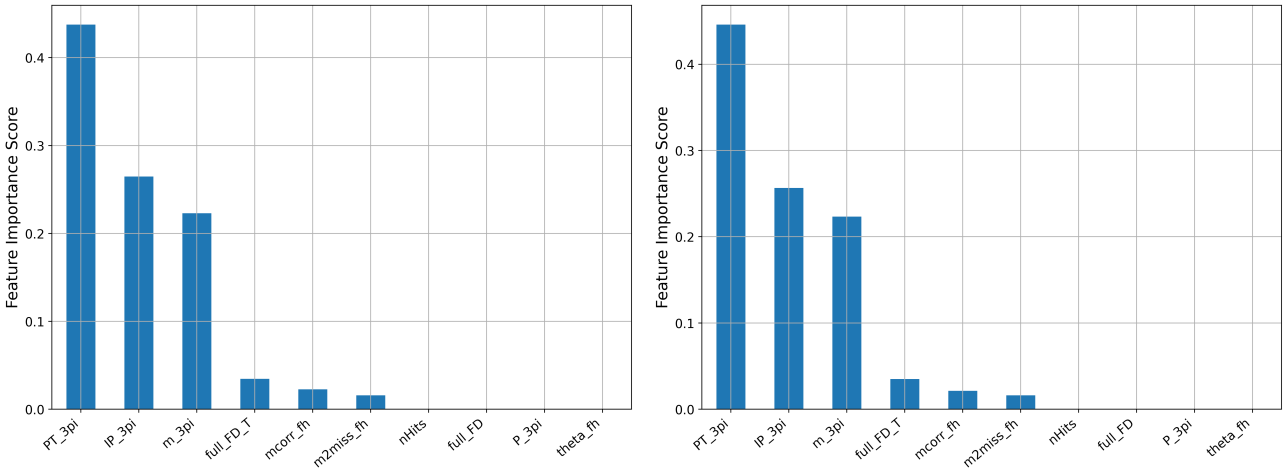

(a) MVA gamma 1 **(b)** MVA gamma 2

Figure 23: Observable importance score of the observables by which the MVA is trained.

The AUC score resulting from MVA gamma 1 and MVA gamma 2 are shown if figure 24. From this figure, it can be seen that both MVA gamma 1 and MVA gamma 2 resulted in an AUC score of 0.927. This result seems to further hint toward a minimal effect for the different $B^+ \to \bar{D}^{0*}\pi^+\pi^+\pi^-$ decay descriptions. For comparison figure 18 shows the AUC score of 0.947 associated with the results of the MC 2000 study shown in figure 17.

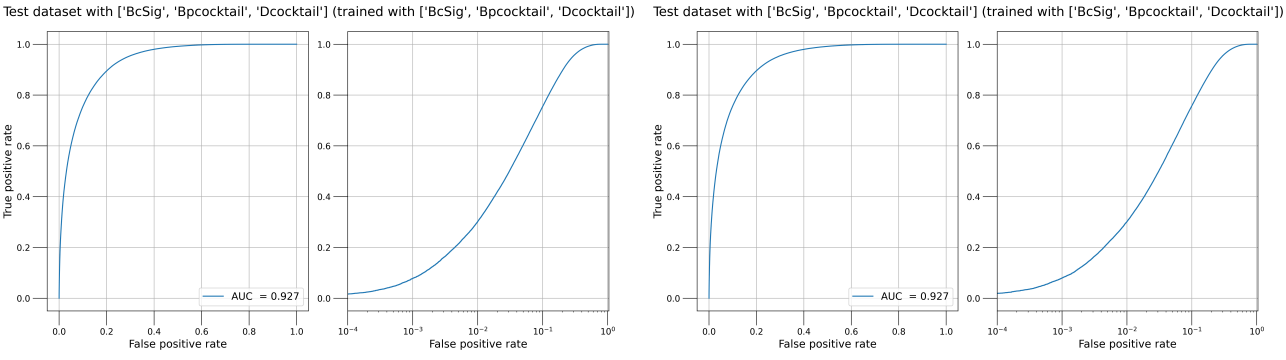

(a) MVA gamma 1 **(b)** MVA gamma 2

Figure 24: Comparison AUC score for MVA gamma 1 (left) and MVA gamma 2 (right).

The result for the MC 2000 study for the MVA gamma 1 and MVA gamma 2 are shown in figure 25 and figure 26 respectively. From these figures, it can be seen that for both MVAs the significance for $B_{cocktial}$ has decreased with roughly 200σ in comparison to the results in figure 17. As the $B_{cocktial}$ includes the

$B^+ \to \bar{D}^0\pi^+\pi^+\pi^-$ and $B^+ \to \bar{D}^{0*}\pi^+\pi^+\pi^-$ decays, this decrease shows that the new description of these decays lowers the MVA capability of distinguishing decays based on the τ resonance structure. The most important result however is the significance of the signal decay. Here, in comparison to the result of 2.94σ shown in figure 17, the significance of the $B_c^+ \to \tau^+\nu_\tau$ decay resulting from MVA gamma 1 has a slight increase of 0.13σ leading to the value of 3.07σ while for MVA gamma 2, there is a decrease of 0.48σ resulting in a significance of 2.46σ. The difference in the significance for the $B_c^+ \to \tau^+\nu_\tau$ decay between MVA gamma 1 and MVA gamma 2, is unexpected as they have the same AUC score and show minimal difference in the spectrum of the observables. This results likely shows that due to the dominant presence of the $B^+ \to \bar{D}^{0*}\pi^+\pi^+\pi^-$ decay in the total number of events, the minimal differences in the observables cause a slight shift in the MVA capability of distinguish the signal decay.

As the difference in the significance for the $B_c^+ \to \tau^+\nu_\tau$ decay between MVA gamma 1 and gamma 2 is roughly 0.5σ, which is a large difference when compared to the significance of the $B_c^+ \to \tau^+\nu_\tau$ decay. It is advised, in order to acquire a more accurate result, to use both the gamma 1 and gamma 2 descriptions of the $B^+ \to \bar{D}^{0*}\pi^+\pi^+\pi^-$ decay.

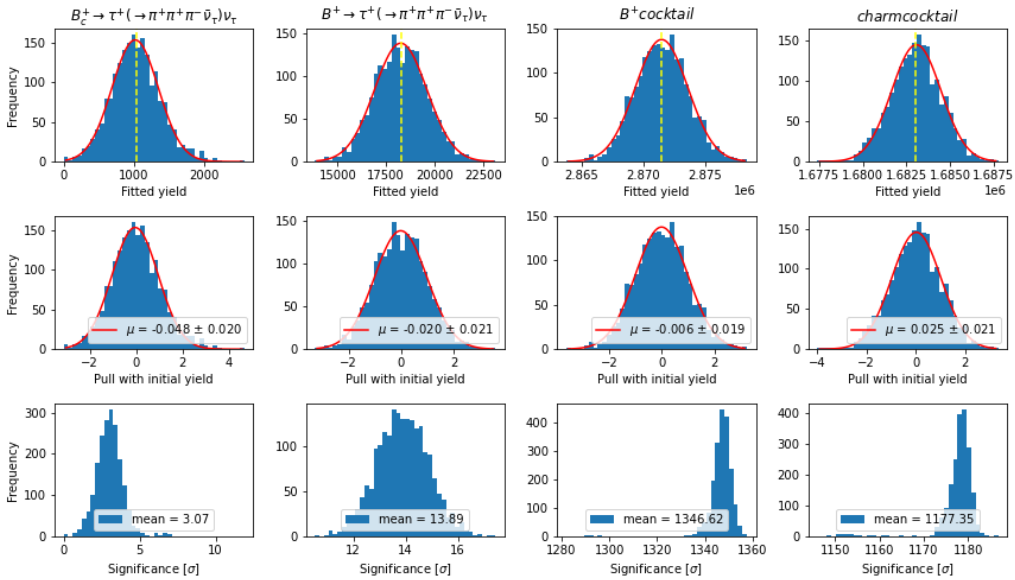

Figure 25: MC 2000 study resulting from MVA gamma 1.

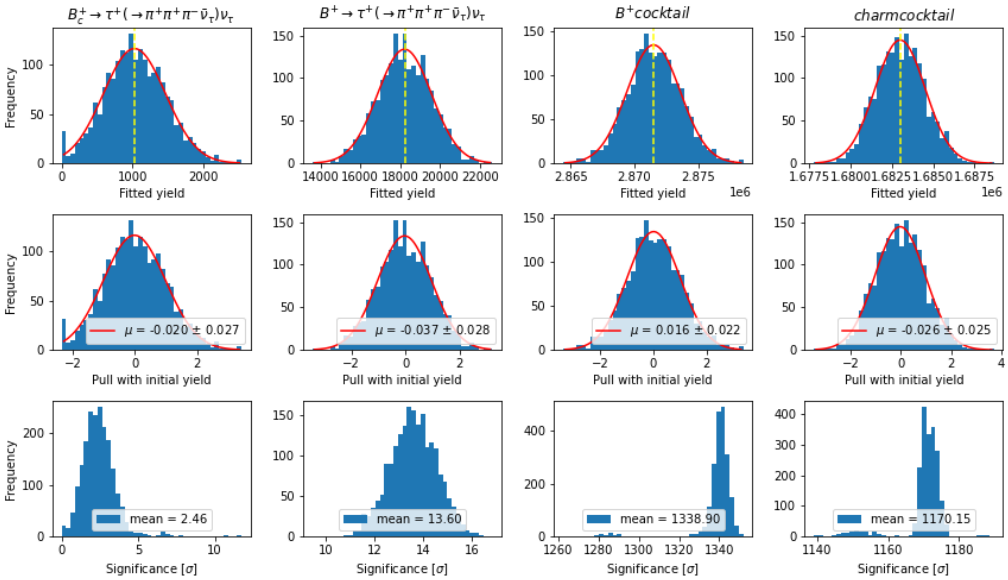

Figure 26: MC 2000 study resulting from MVA gamma 2.

9 Conclusion

In this report the analysis of the $B_c^+ \to \tau^+\nu_\tau$ decay was improved by including the resonance structure of the τ particle and improving the description of the two considered decays that do not include the τ particle, $B^+ \to \bar{D}^0\pi^+\pi^+\pi^-$ and $B^+ \to \bar{D}^{0*}\pi^+\pi^+\pi^-$. Adding these additional structures within the analysis improves the accuracy of the analysis. As within the analysis of the preliminary results, a multivariable analysis is performed (MVA). An MVA allows for a quantification of the accuracy of distinguishing the signal decay from background decays. The MVA acquired from the preliminary results is, in this report, referred to as the original MVA.

The inclusion of the τ resonance structure, in all considered decays that include a τ particle, resulted in a lowering of significance in the signal decay, $B_c^+ \to \tau^+\nu_\tau$, of 0.94σ to the value of 2.57σ when fitted with the original MVA, which was trained on PHSP data. A deviation in the original MVA capability in distinguishing signal decays from background decays was expected as the MVA was optimized for PHSP data. However, when training an MVA with the data that includes the τ resonance structure, the resulting significance for all considered decay is roughly the same with negligible differences. The MVA resulted in a significance of 2.51σ for the signal decay. This result shows that the original MVA performs similarly to an MVA trained on data that includes the τ resonance structure when fitting data that includes the τ resonance structure.

Comparing PHSP data to data that includes the τ resonance structure, shows that the most significant difference is in the spectrum of the mass of the three pions. As this observable is originally not used when training the original MVA, as it proved to have minimal effect on the results, including the resonance structure of the τ particle makes this one of the more important observables for the MVA. Including this observable resulted in an increase in the significance of the signal by roughly 0.5σ to 2.94σ. However, a large fraction of events come from the two decays, namely $B^+ \to \bar{D}^0\pi^+\pi^+\pi^-$ and $B^+ \to \bar{D}^{0*}\pi^+\pi^+\pi^-$, which do not include a τ particle. Because of this, the MVA can distinguish a large fraction of the total number of events by the presence of the resonance structure of the τ particle. This requires that the description of the $B^+ \to \bar{D}^0\pi^+\pi^+\pi^-$ and $B^+ \to \bar{D}^{0*}\pi^+\pi^+\pi^-$ decays also be improved, as the decay channel with the highest branch fraction that makes up these decay also include the a_1 and ρ^0 particle.

As two descriptions for the $B^+ \to \bar{D}^{0*}\pi^+\pi^+\pi^-$ decay where possible, both were used separately with the improved description of the $B^+ \to \bar{D}^0\pi^+\pi^+\pi^-$ decay. This resulted in two MVAs allowing a comparison to be between the descriptions of the $B^+ \to \bar{D}^{0*}\pi^+\pi^+\pi^-$ decay and their effect on the MVA performance. The description of the $B^+ \to \bar{D}^{0*}\pi^+\pi^+\pi^-$ decay deviated from each other in there description of the $\bar{D}^{0*}$ decay. The description referred to as gamma 1 decayed as $\bar{D}^{0*} \to (D^0 \to K^+\pi^-)\gamma$ and the description referred to as gamma 2 decayed as $\bar{D}^{0*} \to (D^0 \to K^+\pi^-)(\pi^0 \to \gamma\gamma)$. The resulting MVAs are referred to as MVA gamma 1 and MVA gamma 2 respectively. The MVAs resulted in a significance for the $B_c^+ \to \tau^+\nu_\tau$ decay of 3.07σ for MVA gamma 1 and 2.46σ for MVA gamma 2. This shows a need to use both descriptions when describing $B^+ \to \bar{D}^{0*}\pi^+\pi^+\pi^-$. When comparing this to the original MVA significance of 3.51σ it shows that the end result of this report resulted in a decrease of the significance for the $B_c^+ \to \tau^+\nu_\tau$ decay of 0.44σ and 1.04σ for MVA gamma 1 and MVA gamma 2 respectively. From this, it can be concluded that improvements are necessary in order to claim the measuring of the $B_c^+ \to \tau^+\nu_\tau$ decay when analyzing real data.

As the improvement made in this report moves the analysis towards real-world conditions, away from approximations, a higher accuracy within the entire analysis is expected. The additions made in this report use the EvtGen and Tauola libraries to generate their event more accurately to real data when compared to the PHSP events generated by RapidSim. EvtGen and Tauola are both MC events simulators that make use of approximation to generate their events within a short time period. These approximations and each library's description of particles have slight differences, causing a small variation in the spectrum of similar particles. As the MVA could possibly use these small variations to distinguish decays that are generated by Tauola from those generated by EvtGen, removing any conflicting approximations or varying descriptions is an important improvement.

References

[1] A. Pais and S. B. Treiman, *How Many Charm Quantum Numbers Are There?*, Phys. Rev. Lett. **35** (1975) 1556.

[2] *The standard model*, Available at: https://home.cern/science/physics/standard-model.

[3] LHCb, R. Aaij *et al.*, *Test of lepton universality with $B^0 \to K^{*0}\ell^+\ell^-$ decays*, JHEP **08** (2017) 055, arXiv:1705.05802.

[4] ATLAS, CMS, LHCb, E. Graverini, *Flavour anomalies: a review*, J. Phys. Conf. Ser. **1137** (2019), no. 1 012025, arXiv:1807.11373.

[5] J. R. de Jong, *Feasibility study of the branching fraction measurements of $b_c^+ \to \tau^+\nu_\tau$ and $b^+ \to \tau^+\nu_\tau$ at lhcb*, .

[6] G. A. Cowan, D. C. Craik, and M. D. Needham, *RapidSim: an application for the fast simulation of heavy-quark hadron decays*, Comput. Phys. Commun. **214** (2017) 239, arXiv:1612.07489.

[7] R. E. Krebs, *Scientific development and misconceptions through the ages: a reference guide*, Greenwood Publishing Group, 1999.

[8] G. Bianco, *Study of the quantum interference between singly and doubly resonant top-quark production in proton-proton collisions at the LHC with the ATLAS detector*, PhD thesis, 12, 2020, doi: 10.13140/RG.2.2.34038.42561.

[9] *Why do physicists mention "five sigma" in their results?*, Available at: https://home.cern/resources/faqs/five-sigma#:~:text=Five%20sigma%20is%20generally%20the,our%20current%20understanding%20of%20nature.

[10] Y. Amhis *et al.*, *Prospects for $B_c^+ \to \tau^+\nu$ at FCC-ee*, JHEP **12** (2021) 133, arXiv:2105.13330.

[11] Particle Data Group, P. A. Zyla *et al.*, *Review of Particle Physics*, PTEP **2020** (2020), no. 8 083C01.

[12] R. Fleischer, R. Jaarsma, and G. Tetlalmatzi-Xolocotzi, *Mapping out the space for new physics with leptonic and semileptonic $B_{(c)}$ decays*, Eur. Phys. J. C **81** (2021), no. 7 658, arXiv:2104.04023.

[13] *Lhcb*, Available at: https://home.cern/science/experiments/lhcb.

[14] LHCb, A. A. Alves, Jr. *et al.*, *The LHCb Detector at the LHC*, JINST **3** (2008) S08005.

[15] K. Hennessy, *LHCb VELO Upgrade*, Nucl. Instrum. Meth. A **845** (2017) 97, arXiv:1604.05045.

[16] LHCb Velo, V. Coco *et al.*, *Velo Upgrade Module Nomenclature*, tech. rep., 2019.

[17] Z. Liu, *What is Cherenkov radiation?*, Jul, 2022. Available at: https://www.iaea.org/newscenter/news/what-is-cherenkov-radiation#:~:text=Cherenkov%20radiation%20is%20a%20form,light%20in%20a%20specific%20medium.

[18] LHCb, R. Aaij *et al.*, *The LHCb upgrade I*, 5, 2023.

[19] LHCb, E. Santovetti, *The LHCb muon detector*, Nucl. Instrum. Meth. A **462** (2001) 297.

[20] *sklearn.ensemble.gradientboostingclassifier*, Available at: https://scikit-learn.org/stable/modules/generated/sklearn.ensemble.GradientBoostingClassifier.html.

[21] *What is overfitting*, Available at: https://www.ibm.com/topics/overfitting.

[22] *Spss kolmogorov-smirnov test for normality*, Available at: https://www.spss-tutorials.com/spss-kolmogorov-smirnov-test-for-normality/?utm_content=cmp-true.

[23] D. J. Lange, *The EvtGen particle decay simulation package*, Nucl. Instrum. Meth. A **462** (2001) 152.

[24] S. Jadach, J. H. Kuhn, and Z. Was, *TAUOLA: A Library of Monte Carlo programs to simulate decays of polarized tau leptons*, Comput. Phys. Commun. **64** (1990) 275.

[25] O. Shekhovtsova, T. Przedzinski, P. Roig, and Z. Was, *Resonance chiral Lagrangian currents and τ decay Monte Carlo*, Phys. Rev. D **86** (2012) 113008, arXiv:1203.3955.

[26] Z. Was and J. Zaremba, *Study of variants for Monte Carlo generators of $\tau \to 3\pi\nu$ decays*, Eur. Phys. J. C **75** (2015), no. 11 566, arXiv:1508.06424, [Erratum: Eur.Phys.J.C 76, 465 (2016)].

[27] I. Nugent *et al.*, *Resonance chiral lagrangian currents and experimental data for τ-$\to$ π- π- $\pi+$ ν τ*, Physical Review D **88** (2013), no. 9 093012.

[28] Working Group on Radiative Corrections, Monte Carlo Generators for Low Energies, S. Actis *et al.*, *Quest for precision in hadronic cross sections at low energy: Monte Carlo tools vs. experimental data*, Eur. Phys. J. C **66** (2010) 585, arXiv:0912.0749.

[29] P. Lichard, *Resonance $a_1(1420)$ and the Three-Pion Decays of the Tauon*, 3, 2017.

A Yield

In table 5 the branching fraction and the number of events used in the PDF are shown for all considered decays.

Decay	$\mathcal{BR}$	**Yield**
$B_c^+ \to \tau^+\nu_\tau$	1.82×10^{-3}	1065
$B^+ \to \tau^+\nu_\tau$	1.015×10^{-5}	18811
$\boldsymbol{D_{cocktail}}$		1732346
$D^+ \to \tau^+\nu_\tau$	1.12×10^{-4}	646382
$D_s^+ \to \tau^+\nu_\tau$	4.95×10^{-3}	1085963
$\boldsymbol{B^+_{cocktail}}$		2955605
$B^+ \to \bar{D}^0\tau^+\nu_\tau$	7.17×10^{-4}	141883
$B^+ \to \bar{D}^{*0}\tau^+\nu_\tau$	1.75×10^{-3}	342555
$B^+ \to \bar{D}^0\pi^+\pi^+\pi^-$	0.0056	850585
$B^+ \to \bar{D}^{0*}\pi^+\pi^+\pi^-$	1.03×10^{-2}	1564469
$B^+ \to \bar{D}^0 D_s^+$	4.45×10^{-5}	15831
$B^+ \to \bar{D}^{0*} D_s^+$	4.06×10^{-5}	14144
$B^+ \to \bar{D}^{0*}(D_s^{*+} \to \gamma D_s^+)$	7.91×10^{-5}	26135

Table 5: Yield and Branching ratios of the considered decays in the analysis. $D_s^+ \to \tau^+\nu_\tau$ is assumed.

B MVA trained on PHSP data with the mass of three pions as observable

An MVA trained with PHSP data, with the additional observables related to the mass of the pions, shows that when the mass of the three pions is included it becomes the most important parameter by which the MVA makes distinctions. This can be seen from figure 27b which shows the feature importance score. Such an MVA results in an AUC score of 0.951 which is an increase of 0.012 when compared to the original MVA which has an AUC score of 0.939. However, the MC 2000 study shows a negligible difference in significance of the $B_c^+ \to \tau^+\nu_\tau$ decay. From this can be concluded that including the mass spectrums of the pions has no significant effect on the MVA capability to distinguish the $B_c^+ \to \tau^+\nu_\tau$ decay.

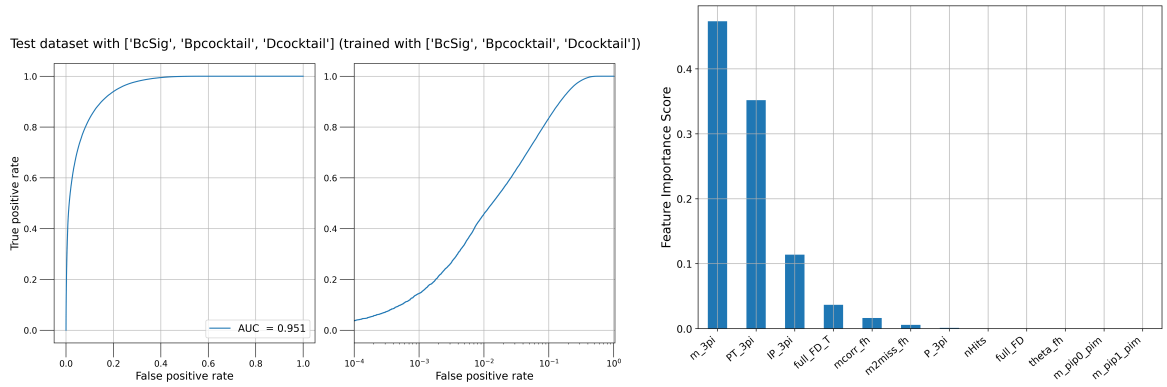

(a) AUC score **(b)** Importance score observables

Figure 27: Resulting AUC score (left) and feature importance score (right) for the MVA trained on PHSP data including the mass of the three pions as observable.

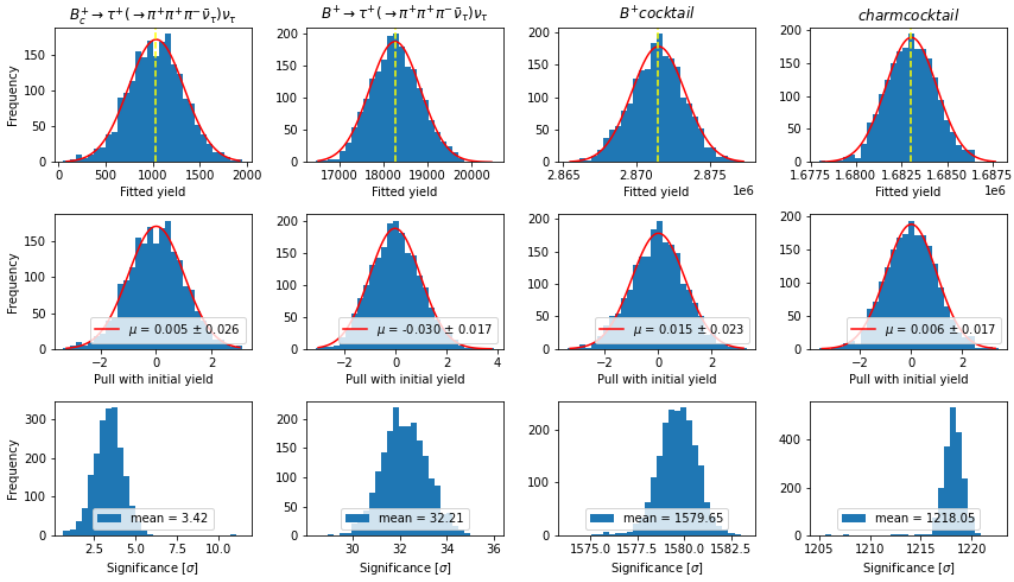

Figure 28: MC 2000 study resulting from the MVA trained on PHSP data including the mass of the three pions as observable.